The Rubredoxin from *Clostridium pasteurianum*: Mutation of the Iron Cysteinyl Ligands to Serine. Crystal and Molecular Structures of Oxidized and Dithionite-Treated Forms of the Cys42Ser Mutant

Zhiguang Xiao,[†] Megan J. Lavery,[†] Mustafa Ayhan,[†] Sergio D. B. Scrofani,[†,‡] Matthew C. J. Wilce,[§] J. Mitchell Guss,*[,§] Peter A. Tregloan,[†] Graham N. George,[⊥] and Anthony G. Wedd*[,†]

Contribution from the School of Chemistry, University of Melbourne, Parkville, Victoria 3052, Australia, Department of Biochemistry, University of Sydney, Sydney, New South Wales 2006, Australia, and Stanford Synchrotron Radiation Laboratory, SLAC, Stanford University, P.O. Box 4349, MS 69, Stanford, California 94309

Received September 9, 1997

Abstract: Isolation is reported of the four mutant proteins of the electron-transfer protein rubredoxin from *Clostridium pasteurianum* in which each of the four cysteine ligands is changed in turn to serine. They fall into two pairs whose properties depend on whether an interior (C6, C39) or a surface (C9, C42) cysteine ligand is substituted. A crystal structure of the oxidized C42S protein (1.65 Å; *R*, 18.5%) confirms the presence of an $Fe^{III}(S^{\gamma}\text{-Cys})_3(O^{\gamma}\text{-Ser})$ center (Fe−O, 1.82(8) Å). Significant structural change is restricted to the region around the mutation. EXAFS experiments confirm $Fe^{III}S_3O$ (O = O^{γ}-Ser or OH_x) centers in each oxidized protein at pH 8. The reduction potentials of the $Fe^{III/II}$ couple are decreased by about 100 and 200 mV, respectively, in the interior and surface ligand mutants. The potentials are pH-dependent with respective pK_a^{red} values of about 9 and 7. EXAFS data indicate an increase of 0.2−0.3 Å in the Fe^{II}−O distances in passing through these characteristic pK_a^{red} values. ^{1}H NMR experiments on Cd^{II} forms reveal the presence of $Cd^{II}(S\text{-Cys})_3\{O(H)\text{-Ser}\}$ centers in the surface ligand mutants C9S and C42S by the detection of $^{113}Cd-O-CH^{\beta}{}_2$ coupling and $S-OH^{\gamma}$ resonances. The assumption of the presence of $Fe^{II}(S\text{-Cys})_3(O\text{-Ser})$ centers in each mutant protein at pH values above the characteristic pK_a^{red} allows a simple interpretation of the electrochemical behavior. Protonation of the $Fe-O^{\gamma}$-Ser link upon reduction is proposed, followed by hydrolysis at lower pH values: $Fe^{III}-O^{\gamma}\text{-Ser} + H^+ + e^- \rightarrow Fe^{II}-O^{\gamma}(H)\text{-Ser}$; $Fe^{II}-O^{\gamma}(H)\text{-Ser} + H_2O \rightarrow Fe^{II}-OH_2 + HO^{\gamma}\text{-Ser}$. The differences in reduction potentials, their pH dependence, and the onset of irreversible electrochemistry can be attributed to differences in the Fe−O bonds of the interior and surface ligands. These differences appear to result from variation in the conformational flexibility of the protein chelate loops which carry the ligands. An attempt to generate crystals of the reduced Fe^{II}-C42S protein by treatment of Fe^{III}-C42S crystals with dithionite at pH 4 led to loss of iron. A crystal structure (1.6 Å; *R*, 16.8%) reveals that cysteine residues 6 and 9 have trapped the oxidation product SO_2, a result confirmed by reactions in solution: $Cys\text{-}SH + SO_2 \rightarrow Cys\text{-}S^{II}-S^{IV}O_2^- + H^+$.

Introduction[1]

The simplest of the iron−sulfur proteins are the rubredoxins (Rd) which feature a single $Fe(S\text{-Cys})_4$ site in a protein of molar mass approximately 6000 Da.[2−5] They are presumed to be electron transport proteins, cycling between ferric and ferrous forms, and this role has been demonstrated in both the sulfate-reducing bacterium *Desulfovibrio gigas* and the aerobe *Pseudomonas oleovorans*.[6,7] The rubredoxin from the dinitrogen-fixing bacterium *Clostridium pasteurianum*, *Cp* Rd, has been examined in some detail. The $Fe(S\text{-Cys})_4$ site and the atoms of the chelate loops (residues 5−11 and 38−44) which carry the cysteine ligands exhibit a *pseudo*-2-fold symmetry which includes six NH···S interactions (Figure 1).[5] It has been expressed in

* To whom correspondence should be addressed. E-mail: T.Wedd@chemistry.unimelb.edu.au; M.Guss@biochem.usyd.edu.au.

[†] University of Melbourne.

[‡] Present address: Department of Molecular Biology, MB2, The Scripps Research Institute, 10550 N. Torrey Pines Rd., La Jolla, CA 92037.

[§] University of Sydney.

[⊥] Stanford University.

(1) Abbreviations used: Asp, aspartate; CAPS, 3-(cyclohexylamino)-1-propanesulfonic acid; CHES, 2-(*N*-cyclohexylamino)ethanesulfonic acid; *Cp*, *Clostridium pasterianum*; CtoS, Cys to Ser; Cys, cysteine; $E°$, standard reduction potential; $E_{1/2}$, reversible midpoint potential; *E.*, *Escherichia*; esd, estimated standard deviation; HiPIP, high potential iron protein; His, histidine; I_p, peak current; K_a, proton dissociation constant; ME, β-mercaptoethanol; MES, 2-(*N*-morpholino)ethanesulfonic acid; MOPS, 3-(*N*-morpholino)propanesulfonic acid; *n*, number of electrons transferred; PAGE, polyacrylamide gel electrophoresis; *Pa*, *Peptococcus aerogenes*; *Pf*, *Pyrococcus furiosus*; Pi, phosphate; r, recombinant; Rd, rubredoxin; σ, estimated standard deviation; Ser, serine; SHE, standard hydrogen electrode; SWV, square wave voltammetry; τ, square wave period; *T*, temperature; Z'_{eff}, effective nuclear charge.

(2) Beinert, H.; Holm, R. H.; Munck, E. *Science* **1997**, *277*, 653−659.

(3) Eaton, W. A.; Lovenberg, W. *Iron−Sulfur Proteins*; Academic Press: New York, 1973; Vol. II, pp 131−162.

(4) Day, M. W.; Hsu, B. T.; Joshua-Tor, L.; Park, J.-B.; Zhou, Z. H.; Adams, M. W. W.; Rees, D. C. *Protein Sci.* **1992**, *1*, 1494−1507.

(5) Sieker, L. C.; Stenkamp, R. E.; LeGall, J. *Methods Enzymol.* **1994**, *243*, 203−216.

(6) Santos, H.; Faraleira, P.; Xavier, A. V.; Chen, L.; Liu, M.-Y.; Le Gall, J. *Biochem. Biophys. Res. Commun.* **1993**, *195*, 551−557.

(7) Eggink, G.; Engel, H.; Vriend, G.; Terpastra, P.; Witholt, B. *J. Mol. Biol.* **1990**, *212*, 135−142.

S0002-7863(97)03162-4 CCC: $15.00
Published on Web 04/17/1998

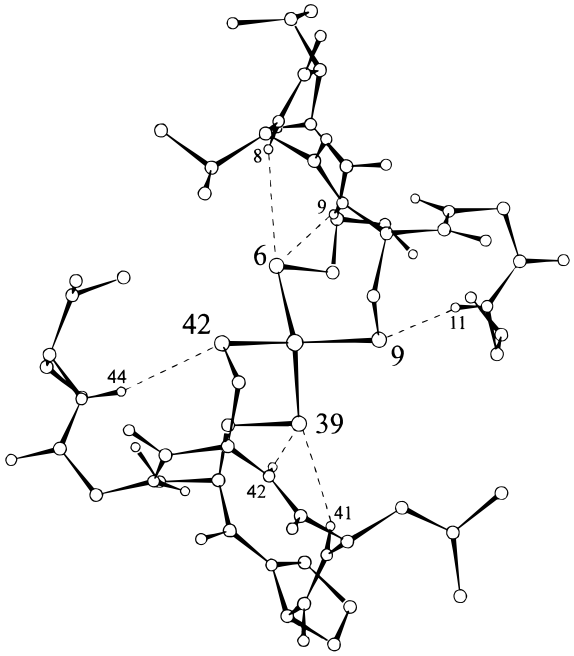

Figure 1. NH···S interactions (- - -) around the Fe(S-Cys)$_4$ center in *Cp* Rd (generated from the coordinates of pdb5rxn.ent in the Brookhaven Protein Databank). The pseudo-2-fold axis (see the text) is perpendicular to the page, passing though the Fe atom.

Escherichia coli, providing ample recombinant protein, *Cp* rRd.[8−10] Generation of mutant forms has begun.[10−13]

The reduction potential of a protein active site is determined by its ionization energy, governed by electronic structure, and by its "solvation energy", which accounts for reorganization of the active site environment upon reduction.[14] The present work has generated mutant proteins C6S, C9S, C39S, and C42S[11] of *Cp* rRd in which each of the four cysteine ligands has been replaced, in turn, by serine. Four geometric isomers have been created in which $FeOS_3$ centers are orientated differently within the same protein chain. The system provides an excellent opportunity for systematic exploration of the factors determining reduction potential.

The orientation of peptide amide and side chain dipoles (including NH···S hydrogen-bonding interactions) and access of solvent water to the active site are proposed to influence the solvation energy term for iron−sulfur proteins.[15−17] These electrostatic interactions tune the potential of a given center. Surface charges are important in some systems but not in others, a variation which may be related to the influence of solvent water in damping charge effects.[13,17−21]

Iron−sulfur centers in proteins are usually bound to the protein chain by Fe−S-Cys links.[22] Nitrogen (His) and oxygen (Asp, OH_x) ligands are confirmed to be present in a number of systems[23−27] and may be present in others.[28] However, while the side chain of serine is identified as a ligand in a number of metalloproteins (cf. dimethyl sulfoxide reductase[29]), it may be disfavored in iron−sulfur proteins by the significantly lower FeO bond strength and by the energy penalty inherent in deprotonating Ser (pK_a, 13.6) relative to more acidic ligands.[30] When presented with a choice, the Fe_4S_4 cluster of ferredoxin I in *Azotobacter vinelandii* prefers Cys over Ser as a ligand.[31]

In fact, Ser has been identified as a ligand in a single iron−sulfur system only: Ser$^{\beta 188}$ with Cys$^{\beta 153}$ binds to one of the iron atoms (Fe−O$^{\gamma}$, 2.0 Å) in the oxidized state of the Fe_8S_7 "P-cluster" of the iron−molybdenum protein of nitrogenase.[32] The amide nitrogen of Cys$^{\alpha 88}$ is the only other non-cysteinyl ligand. Upon reduction by two electrons, the two non-cysteinyl ligands are replaced by Fe−S interactions involving a cluster sulfide. Both the unbound Ser and amide ligands will be protonated in the reduced state and may be deprotonated when bound in the oxidized state. This suggests a possible mechanism for correlated ($2e^-$, $2H^+$) transfer between the P-cluster and the catalytic reducing center, the iron−molybdenum cofactor.[32]

Ser for Cys substitution in iron−sulfur proteins via site-directed mutagenesis has been used widely for identification of ligands and for creating new coordination environments.[23,30,33−37] In many cases, the substitution leads to loss or modification of the iron−sulfur center. For example, only

(8) Mathieu, I.; Meyer, J.; Moulis, J.-M. *Biochem. J.* **1992**, *285*, 255−262.
(9) Eidness, M. K.; O'Dell, J. E.; Kurtz, D. M., Jr.; Robson, R. L.; Scott, R. A. *Protein Eng.* **1992**, *5*, 367−371.
(10) Ayhan, M.; Xiao, Z.; Lavery, M. J.; Hamer, A. M.; Nugent, K. W.; Scrofani, S. D. B.; Guss, M.; Wedd, A. G. *Inorg. Chem.* **1996**, *35*, 5902−5911.
(11) (a) Meyer, J.; Gaillard, J.; Lutz, M. *Biochem. Biophys. Res. Commun.* **1995**, *212*, 827−833. (b) Meyer, J.; Gagnon, J.; Gaillard, J.; Lutz, M.; Achim, C.; Munck, E.; Petillot, Y.; Colangelo, C. M.; Scott, R. A. *Biochemistry* **1997**, *36*, 13374−13380.
(12) Richie, K. A.; Teng, Q.; Elkin, C. J.; Kurtz, D. M., Jr. *Protein Sci*. **1996**, *5*, 883−894.
(13) Zeng, Q.; Smith, E. T.; Kurtz, D. M., Jr.; Scott, R. A. *Inorg. Chim. Acta* **1996**, *242*, 245−251.
(14) Holm, R. H.; Kennepohl, P.; Solomon, E. I. *Chem. Rev.* **1996**, *96*, 2239−2314.
(15) Backes, G.; Mino, Y.; Loehr, T. M.; Meyer, T. E.; Cusanovich, M. A.; Sweeney, W. V.; Adman, E. T.; Sanders-Loehr, J. *J. Am. Chem. Soc.* **1991**, *113*, 2055−2064.
(16) Stephens, P. J.; Jollie, D. R.; Warshel, A. *Chem. Rev.* **1996**, *96*, 2491−2513.
(17) Swartz, P. D.; Beck, B. W.; Ichiye, T. *Biophys. J.* **1996**, *71*, 2958−2969.
(18) Banci, L.; Bertini, I.; Savellini, G. G.; Luchinat, C. *Inorg. Chem.* **1996**, *35*, 4248−4253.
(19) Bertini, I.; Bosari, M.; Bosi, M.; Eltis, D.; Felli, I. C.; Luchinat, C.; Piccioli, M. *J. Biol. Inorg. Chem.* **1996**, *1*, 257−263.
(20) Moulis, J.-M.; Davasse, V. *Biochemistry* **1995**, *34*, 16781−16788.
(21) Brereton, P. B.; Lavery, M. J.; Tregloan, P. A.; Wedd, A. G., submitted for publication.
(22) Johnson, M. K. In *Encyclopedia of Inorganic Chemistry*; King, R. B., Ed.; Wiley: New York, 1994; Vol. 4, pp 1896−1915.
(23) Moulis, J.-M.; Davasse, V.; Golinelli, M.-P.; Meyer, J.; Quinkal, I. *J. Biol. Inorg. Chem.* **1996**, *1*, 2−14, and references therein.
(24) Volbeda, A.; Charon, M.-H.; Piras, C.; Hatchikian, E. C.; Frey, M.; Fontecilla-Camps, J. C. *Nature* **1995**, *373*, 580−587.
(25) Calzolai, L.; Zhou, Z. H.; Adams, M. W. W.; La Mar, G. N. *J. Am. Chem. Soc.* **1996**, *118*, 2513−2514.
(26) Busch, J. L. H.; Breton, J. L.; Bartlett, B. M.; Armstrong, F. A.; James, R.; Thomson, A. J. *Biochem. J.* **1997**, *323*, 95−102 and references therein.
(27) Beinert, H.; Kennedy, M. C.; Stout, C. D. *Chem. Rev.* **1996**, *96*, 2335−2373.
(28) (a) George, S. J.; Armstrong, F. A.; Hatchikian, E. C.; Thomson, A. J. *Biochem. J.* **1989**, *264*, 275−284 (b) Meyers, J.; Fujinga, J.; Gaillard, J.; Lutz, M. *Biochemistry* **1994**, *33*, 13642−13650. (c) Yu, L.; Bryant, D. A.; Golbeck, J. H. *Biochemistry* **1995**, *34*, 7861−7868. (d) Yu, L.; Vassiliev, I. R.; Yung, Y.-S.; Bryant, D. A.; Golbeck, J. H. *J Biol. Chem.* **1995**, *270*, 28118−28125.
(29) Schindelin, H.; Kisker, C.; Hilton, J.; Rajagopalan, K.. V.; Rees, D. C. *Science* **1996**, 272, 1615−1621.
(30) Xia, B.; Cheng, H.; Bandarian, V.; Reed, G. H.; Markley, J. L. *Biochemistry* **1996**, *35*, 9488−9595.
(31) Shen, B.; Jollie, D. R.; Stout, C. D.; Stephens, P. J.; Burgess, B. K.*Proc. Natl. Acad. Sci. U.S.A.* **1995**, *92*, 10064−10068.
(32) (a) Kim, J.; Rees, D. C. *Science* **1992**, *257*, 1677−1682. (b) Peters, J. W.; Stowell, M. H. B.; Soltis, S. M.; Finnegan, M. G.; Johnson, M. K.; Rees, D. C. *Biochemistry* **1977**, *36*, 1181−1187.8
(33) Meyer, J.; Fujinaga, J.; Gaillard, J.; Lutz, M. *Biochemistry* **1994**, *33*, 13642−13650.
(34) Uhlmann, H.; Bernhardt, R. M. *J. Biol. Chem.* **1995**, *270*, 29959−29966.
(35) Kowal, A. T.; Werth, M. T.; Manodori, A.; Cecchini, G.; Schroder, I.; Gunsalus, R.; Johnson, M. K. *Biochemistry* **1995**, *34*, 12284−12293.
(36) Achim, C.; Golinelli, M.-P.; Bominaar, E. L.; Meyer, J.; Munck, E. *J. Am. Chem. Soc.* **1996**, *118*, 8168−8169.

Table 1. Primer Oligonucleotides

mutant	
C6S	5′-CACATACTGTA**G**ATGTATACTTC-3′
C9S	5′-AAATATATCCA**G**ATACTGTACATG-3′
C39S	5′-CACACAAAGGA**G**ATACCCAATC-3′
C42S	5′-TCCTACTCCA**G**ACAAAGGACA-3′

the C77S mutant of the high potential iron protein (HiPIP) from *Chromatium vinosum* retains its Fe_4S_4 center.[38] ^{1}H NMR structural and related studies indicate that the serine side chain is coordinated as the alkoxide in both the oxidized and reduced forms (Fe−O$^\gamma$, 2.3 ± 0.6 Å).[38b] A serine ligand is present in each of the four Cys to Ser mutant forms of the oxidized Fe_2S_2-ferredoxin from an *Anabaena* species,[37] and an Asp to Ser ligand mutation is stable in the Fe_4S_4-ferredoxin from *Pyrococcus furiosus*.[39]

In the present work, the effect of systematic monosubstitution of O for S in the Fe(S-Cys)$_4$ coordination sphere of *Cp* Rd is examined. The properties of the four mutant proteins fall into pairs reflecting the pseudo-2-fold symmetry around the active site of the native protein (Figure 1). The effect on the reduction potential is dramatic, with shifts of up to 200 mV. In addition, a pH dependence of the potential is induced in each protein. The structural basis for these changes is explored by X-ray crystallography and X-ray absorption spectroscopy.

Experimental Section

General materials and DNA manipulations have been described previously.[10] Oligonucleotides were synthesized on an Applied Biosystems DNA synthesizer, model 380A.

Mutagenesis. Techniques have been described previously.[10] The primers used for the four mutants are listed in Table 1. The boldface bases are mismatched and convert the cysteine codon to serine. After mutagenesis and identification by DNA sequencing, the four mutants (C6S, C9S, C39S, C42S) were subcloned into the *Eco*RI and *Pst*I sites of the pKK223-3 vector for protein expression.

Protein Expression and Reconstitution. Plasmids pKK223-3/*Cp* Rd carrying the four mutations were transformed into *E. coli* strain JM109. The procedures for protein expression were similar to those described previously.[10] Each of the four genes was expressed as a colorless protein. The C6S example was purified by the following procedure. After 2-fold dilution with buffer (Tris−HCl; 50 mM; pH 7.4), the crude lysate was applied to a DE-52 column and the absorbed proteins eluted with a NaCl gradient (0.1−0.4 M buffer). The fraction eluting at [NaCl] = 0.21−0.27 M contained the Rd mutant, as identified by SDS−PAGE. This fraction was bound to a second DE-52 column and the protein eluted as above. The eluate was concentrated using an Amicon ultrafiltration cell equipped with a YM3 membrane and treated with $(NH_4)_2SO_4$ to 60% saturation. After removal of precipitate, the supernatant was concentrated further and desalted on a G-25 gel filtration column (1.2 × 75 cm) with distilled water. The protein was identified as a mixture of the Zn^{II} (>90%) and apo (<10%) forms of the C6S mutant by electrospray mass spectroscopy (Figure 2 and Table 2).

The Zn forms of the mutant proteins can be reconstituted readily with iron. The most convenient point for reconstitution is the crude cell lysate stage as the subsequent purification steps are simplified.

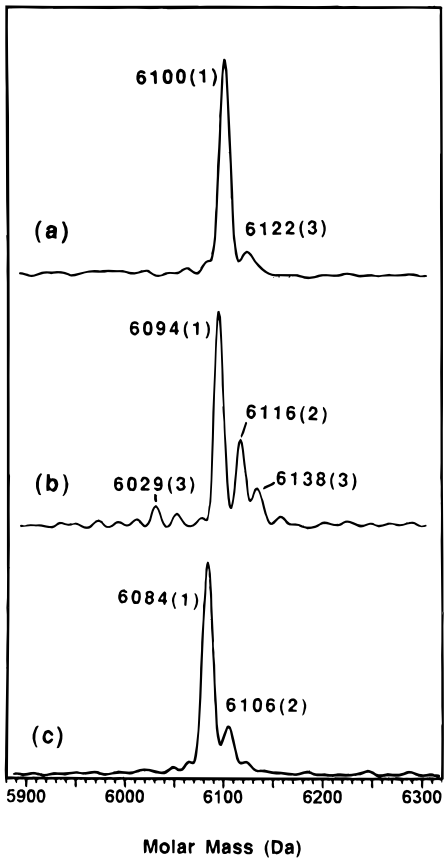

Figure 2. Negative-ion electrospray ionization mass spectra of *Cp* Rd proteins: (a) recombinant; (b) Zn^{II}-C6S as isolated; (c) Fe^{III}-C6S as reconstituted. The proteins (0.2−1.0 mM) suspended in distilled water were infused into a mixture of MeOH−H_2O−Et_3N (30:70:0.1 v/v/v). Weak peaks with higher molar masses are due to the formation of Na^+−protein adducts.

Table 2. Molar Masses (Da) Determined by Electrospray Mass Spectrometry[a]

Cp Rd	calculated	found[b]
recombinant	6100.5	6100(1)
Zn^{II}−C6S[c]	6094.5	6095(1)
Fe^{III}-C6S/C9S/C39S/C42S	6084.4	6084(1)
apo-C6S/C9S/C39S/C42S	6031.6	6029(1)
Co^{II}-C6S/C9S/C39S	6088.5	6091(1)
$^{113}Cd^{II}$-recombinant	6158.7	6159(1)
$^{113}Cd^{II}$-C6S/C39S	6142.1	6142(1)
Products from Treatment of Fe^{III}-C42S Protein with Dithionite at pH 4		
apo(SS, SH)[d]	6029.5	6029(1)[e]
apo(SS, SSO_2^-)[f]	6093.6	6094(1)[g]
apo(SH, $2SSO_2^-$)[h]	6159.7	6158(1)[i]

[a] Determined under basic conditions in negative ion mode; mobile phase: H_2O/MeOH/Et_3N = 70/30/0.1 v/v/v. [b] Single standard deviations given in parentheses. [c] As isolated. [d] Apo-C42S protein with one cystine disulfide link and one Cys-SH residue. [e] Peaks at *m*/*e* 6051 and 6074 are assigned to adducts of apo(SS, SH) with 1 Na^+ and 2 Na^+ ions. [f] Apo-C42S protein with one cystine disulfide link and one modified Cys-SSO_2^- residue. [g] Peaks at *m*/*e* 6116 and 6138 are assigned to adducts of apo(SS, SSO_2^-) with 1 Na^+ and 2 Na^+ ions. [h] Apo-C42S protein with one Cys-SH and two modified Cys-SSO_2^- residues. [i] A peak at *m*/*e* 6179 is assigned to an adduct of apo(SH, $SSSO_2^-$) with 1 Na^+ ion.

The procedure was derived from that described earlier.[40] The protein in the crude lysate was precipitated by addition of trichloroacetic acid

(37) Holden, H. M.; Jacobson, B. L.; Hurley, J. K.; Tollin, G.; Oh, B. H.; Skjeldahl, L.; Chae, Y. K.; Cheng, H.; Xia, B.; Markley, J. L. *J. Bioenerg. Biomembr.* **1994**, *26*, 67−88.

(38) (a) Argawal, A.; Li S.; Cowan, J. A. *J. Am. Chem. Soc.* **1996**, *118*, 8, 926−928. (b) Bentrop, D.; Bertini, I.; Capozzi, F.; Dikiy, A.; Eltis, D.; Luchinat, C. *Biochemistry* **1996**, *35*, 5928−5936.

(39) Calzolai, L.; Gorst, C. M.; Bren, K. L.; Zhou, Z.-H.; Adams, M. W. W.; La Mar, G. N. *J. Am. Chem. Soc.* **1997**, *119*, 9341−9350.

(40) (a) Lovenberg, W.; Williams, W. M. *Biochemistry* **1969**, *8*, 141−153. (b) Moura, I.; Teixeira, M.; LeGall, J.; Moura, J. J. G. *J. Inorg. Biochem.* **1991**, *44*, 127−139.

(20% in water) and β-mercaptoethanol (ME) to final concentrations of ca. 5−10% and 0.3−0.5 M, respectively. After centrifugation and removal of the supernatant, the precipitate was washed with a mixture of 5% trichloroacetic acid and 50 mM ME and extracted 2−3 times with Tris base (0.5 M; 1−2 mL/g of cells) containing ME (0.5 M). Insoluble material was discarded, and the extracts were combined. The protein was reprecipitated, washed, and redissolved as detailed above to minimize contamination by Zn^{II} and other metal ions. A 5-fold excess of $Fe(NO_3)_3$ (0.2 M) was added, producing an orange solution whose color faded with concomitant formation of green insoluble material. After incubation on ice for 1 h, the green precipitate was removed by filtration. After ca. 5-fold dilution with water, the orange color reappeared, and the solution was applied to a DE-52 column (3.3 × 12 cm). The protein was eluted with a NaCl gradient (0.10−0.30 M) in Tris−HCl buffer (50 mM; pH 7.4) at a flow rate of 40 mL h^{-1}. For each mutant, an intense orange band was observed. Fractions with $A_{280}/A_{350} \leq 3$ for C6S and C39S and with $A_{280}/A_{335} \leq 3$ for C9S and C42S were combined and treated with ammonium sulfate to 60% saturation. After several hours, the precipitate was discarded and the supernatant applied to a Phenyl Sepharose CL-4B column (2.8 × 13 cm) equilibrated with 50% saturation ammonium sulfate in KP_i buffer (50 mM; pH 7.5). The orange protein was eluted with a 50−0% saturation ammonium sulfate gradient in the phosphate buffer at a flow rate of 40 mL h^{-1}. Fractions with $A_{280}/A_{350} \leq 1.8$ for C6S, $A_{280}/A_{336} \leq 1.8$ for C9S, $A_{280}/A_{345} \leq 1.9$ for C39S, and $A_{280}/A_{331} \leq 1.7$ for C42S, respectively, were pooled and concentrated by ultrafiltration. Yields were around 10 mg L^{-1} of starting culture for each mutant. The samples were >95% pure as judged by SDS−PAGE and electrospray mass spectrometry. The first 12 amino acids of the C6S and C9S proteins were confirmed by sequential Edman degradation.

Physical Measurements. Electronic spectra, electrospray ionization mass spectra and resonance Raman spectra, were obtained as described previously.[10] EPR spectra were recorded on an X-band EPR spectrometer (Bruker ESP380E) with an Oxford Instruments helium flow cryostat: standard, 1,1-diphenyl-2-picrylhydrazyl; modulation frequency, 100 kHz; modulation amplitude, 0.2 mT; microwave power, ca. 0.5 mW; temperature, 4.2 K. The samples (ca. 0.2 mL) were 1.6 mM in protein, 50 mM in Tris−HCl buffer (pH, 7.4), and 150 mM in NaCl. D_2O samples were prepared by freeze-drying the above samples followed by redissolution in D_2O. Electronic spectra before and after the drying procedure were indistinguishable.

Electrochemistry. Electrochemical experiments were carried out at 25 ± 1 °C in a water-jacketed cell whose temperature was controlled with a circulating water bath. A standard three-electrode system was used. The working electrode was a disk (*d*, 5 mm) of edge-cleaved pyrolytic graphite (Le Carbone-Lorraine) housed in a sheath of epoxy resin. The electrode was polished manually using a slurry of alumina (0.3 μm) in water and rinsed with distilled water. The counter electrode was a Pt wire. Reduction potentials are quoted relative to SHE and were measured via a KCl-saturated Ag/AgCl reference electrode (potential, 199 mV vs SHE at 25 °C). All electrochemical data were acquired by square wave voltammetry (SWV).[41,42] Equilibrium reduction potentials were read directly from the current peak potential of the voltammograms. The number of electrons transferred (*n*) was determined from the width at half-height (126 mV/*n*). About 500 μL of protein solution (100 μM) in buffer (30 mM) and NaCl (100 mM) were used for each experiment. Each sample was derived by dilution of a protein stock solution (3−5 mM) in Tris−HCl (30 mM; pH 7.4) with the appropriate buffer at the required pH. Buffers (pK_a) used were acetic acid (4.7), MES (6.1), MOPS (7.2), tricine (8.1), CHES (9.3), and CAPS (10.4). Each buffer was adjusted with NaOH to the appropriate pH near its pK_a to maximize the buffer capacity and minimize variation of the ionic strength. Control experiments showed that a maximum change in buffer pH upon addition of a required amount of stock protein solution was less than 0.05 pH unit. Poly(L-lysine) (100 μM) was used as promoter: a correction of +9 mV was applied for the induced shift in potential.[10,43] Before each measurement, dioxygen was removed by bubbling water-saturated dinitrogen through the solution. Anaerobic conditions were maintained by passing dinitrogen over the surface of the solution.

Reversibility and reproducibility of the electrode responses of each mutant were found to be dependent on the pH of the solution. At pH 6−10 for C9S and C42S, and pH 7.6−10.5 for C6S, the responses were chemically reversible and reproducible but became irreversible or showed no response at lower pH. The reported reduction potential at each pH is the averaged value of at least three successive scans for a reversible response or of three first scans, each after polishing the electrode surface, for an irreversible response.

NMR of ^{113}Cd-Substituted Samples. The recombinant wild type and four cysteine to serine mutants were reconstituted with ^{113}Cd for NMR investigations. The procedures employed purified Fe^{III} forms and followed those outlined previously.[10]

Unless otherwise specified, all ^{1}H and ^{113}Cd NMR data were collected at 303 K with samples containing ^{113}Cd-substituted Rd (5 mM), NaCl (200 mM), and phosphate buffer (20 mM; pH 6.8) in 90% H_2O/10% D_2O. Two-dimensional experiments included DQF-COSY,[44] DQ-COSY,[45,46] NOESY,[47] and TOCSY.[48] They were recorded on a Bruker DRX 500 spectrometer, operating at 500 MHz for ^{1}H, over a spectral width of 8013 Hz. A total of 512−768 t_1 increments of 2048 real points using either States-TPPI or TPPI was used for quadrature detection.[49,50] Water suppression was achieved using either the SCUBA sequence[51] or low-powered irradiation during the recycle delay. DQ-COSY experiments were acquired with a DQ preparation period of 30 ms. TOCSY spectra (40−90 ms) were acquired using the MLEV-17 mixing scheme, flanked by 2.5 ms trim pulses. For NOESY spectra, mixing times of 100−250 ms were utilized. DQF-COSY experiments were acquired with 4096 data points and 1024 t_1 increments.

^{113}Cd NMR spectra were acquired on a Varian Unity-Plus 400 NMR spectrometer (88.72 MHz for ^{113}Cd). One-dimensional {^{1}H−^{113}Cd} HMQC spectra were acquired at 400 MHz with evolution periods of 12.5−70 ms (40−7 Hz).[52,53] Typically, 5000−30000 transients were required for detection of NH···S donors. GARP decoupling was applied during acquisition.[54]

Two-dimensional data were processed using either Bruker XWIN NMR software or Varian VNMR 5.1 software. For NOESY and TOCSY spectra, 60−80° shifted square sine bells were typically used in both dimensions and zero-filled to a final matrix size of 4096 × 2048 real data points. $^3J_{N_H\alpha}$ coupling constants for ^{113}Cd−*Cp* rRd were determined from DQF-COSY experiments, zero-filled to 8192 × 2048 real data points, and evaluated by the method of Kim and Prestegard.[55] Proton chemical shifts were referenced to the H_2O signal at 4.73 ppm (303 K), and ^{113}Cd resonances were referenced indirectly to $Cd(ClO4)_2$ (0.0 ppm, 0.1 M).

(41) (a) Christie, J. H.; Turner, J. A.; Osteryoung, R. A. *Anal. Chem.* **1977**, *49*, 1899−1903. (b) Turner, J. A.; Christie, J. H.; Vukovic, M.; Osteryoung, R. A. *Anal. Chem.* **1977**, *49*, 1904−1908. (c) O'Dea, J. J.; Osteryoung, J.; Osteryoung, R. A. *Anal. Chem.* **1981**, *53*, 695−701.

(42) Smith, E. T.; Feinberg, B. A. *J. Biol. Chem.* **1990**, *265*, 14371−14376.

(43) Lavery, M. J.; Xiao, Z.; Bond, A. M.; Wedd, A. G. Submitted for publication.

(44) Rance, M.; Sørensen, O. W.; Bodenhausen, G.; Wagner, G.; Ernst, R. R.; Wüthrich, K. *Biochem. Biophys. Res. Commun.* **1983**, *117*, 479−485.

(45) Braunschweiler, L.; Bodenhausen, G.; Ernst, R. R. *Mol. Phys.* **1983**, *48*, 535−560.

(46) Rance, M.; Chazin, W. J.; Dalvit, C.; Wright, P. E. *Methods Enzymol.* **1989**, *176*, 114.

(47) Macura, S.; Ernst, R. R. *Mol. Phys.* **1980**, *41*, 95−117.

(48) Bax, A.; Davis, D. G. *J. Magn. Reson.* **1985**, *63*, 207−213.

(49) Marion, D.; Ikura, M.; Tschudin, R.; Bax, A. *J. Magn. Reson.* **1989**, *85*, 393−399.

(50) Marion, D.; Wüthrich, K. *Biochem. Biophys. Res. Commun.* **1983**, *113*, 967−974.

(51) Brown, S. C.; Weber, P. L.; Mueller, L. *J. Magn. Reson.* **1988**, *77*, 166−169.

(52) Bax, A.; Griffey, R. G.; Hawkins, B. L. *J. Am. Chem. Soc.* **1983**, *105*, 7188−7190.

(53) Bax, A.; Griffey, R. G.; Hawkins, B. L. *J. Magn. Reson.* **1983**, *55*, 301−315.

(54) Shaka, A. J., Barker, P. B., Freeman, R. *J. Magn. Reson.* **1985**, *64*, 547−552.

(55) Kim, Y.; Prestegard, J. H. *J. Magn. Reson.* **1989**, *84*, 9−13.

X-ray Crystallography. The structures of the C42S mutant protein in oxidized and dithionite-reduced forms were solved by single-crystal X-ray diffraction.

Crystallization. The highly acidic nature of *Cp* Rd (pI ≈ 4) means that the solubility of the protein is low at pH ≈ 4. The conditions reported for the original crystallization (pH 4.0; ammonium sulfate, 75% of saturation) were used as a basis for hanging drop vapor diffusion experiments.[56] Optimal crystallization of Fe^{III}-C42S occurred in 8 μL drops containing protein (0.8 mM), ammonium sulfate (25−30%), and sodium acetate buffer (50 mM; pH 4.0). These were equilibrated against a 700 μL reservoir containing ammonium sulfate (50−60%) in the same buffer. Overnucleation occurred, but single crystals were present. To collect high-resolution data, a dark orange crystal of dimensions 0.38 × 0.23 × 0.15 mm was chosen and mounted in a capillary in the presence of a drop of mother liquor.

Crystals of Fe^{III}-C42S were reduced with sodium dithionite. A crystal (approximate dimensions 0.2 × 0.2 × 0.1 mm) was mounted in a drop of mother liquor in a capillary (*d*, 0.7 mm) in the presence of air. A second drop of mother liquor, saturated with dithionite, was placed next to the first drop, and the end of the capillary was immediately sealed with wax. A few grains of sodium dithionite, on the end of a glass fiber wetted with mother liquor, were added to the drop containing the crystal. The crystal bleached and was pushed with a glass fiber into the gas bubble separating the two drops. The other end of the capillary was sealed immediately.

Data Collection. X-rays were generated by a Rigaku RU-200 rotating anode (Cu Kα; λ, 1.5418 Å), focused with mirrors and filtered with a nickel foil. All data were recorded at 293 K, for a single crystal each of the oxidized and reduced forms. The images were collected on an R-AXIS imaging plate scanner. Two sets of data were recorded from a single crystal of the Fe^{III}-C42S protein (0.4 × 0.2 × 0.15 mm) in two passes. The first pass, 15 min of exposure and 0.000 15 in. Ni foil, was chosen to optimize the exposure of the high angle reflections. The second one, 10 min of exposure and 0.000 25 in. Ni foil, was made to measure the low angle reflections overexposed in the first pass. Nonoverlapping frames were recorded on each pass at room temperature with the same crystal−film distance (70 mm), oscillation angle $\Delta\phi$ (1.7°), and number of frames collected (32). For dithionite-reduced C42S protein, a crystal of dimensions 0.2 × 0.1 × 0.1 mm was used to record the data with a crystal−film distance of 65 mm and $\Delta\phi$ value of 3° for a total of 20 frames (exposure time 10 min/image and 0.000 15 in. Ni foil). The crystal remained colorless throughout the data collection. Derived parameters for each crystal are listed in Table 3.

The intensities were integrated, scaled, and merged using the program DENZO.[57] Data for each crystal extended to good resolution with adequate completeness. Both forms of Rd *Cp* C42S crystallized in space group *R*3 and were isomorphous with the native protein.

Refinement. The starting model in each case was the 5RXN entry for *Cp* Rd in the Protein Data Bank with the water atoms removed. Refinement of the models for both structures was achieved using the CCP4 suite of programs.[58] The models were refined using the program PROLSQ.[59] *R*-free validation was used on the basis of a subset of 5% of the reflections. The positions of water molecules in the structure were identified by inspection of the $2F_o - F_c$ and $F_o - F_c$ electron density maps. The final list of water molecules was further confirmed by examining omit maps calculated with contributions from blocks of water molecules omitted from the structure factor calculations. Model building and visualization were achieved using the program O.[60]

(56) Herriott, J. R.; Sieker, L. C.; Jensen, L. H.; Lovenberg, W. *J. Mol. Biol.* **1970**, *50*, 391−406.
(57) Otwinowski, Z.; Minor, W. *DENZO: A Film Processing Program for Macromolecular Crystallography*; Yale University: New Haven, CT, 1993.
(58) Collaborative Computational Project, Number 4. *Acta Crystallogr.* **1994**, *D50*, 760−763.
(59) Konnert, J. H.; 4 Hendrickson W. A. *Acta Crystallogr. A* **1980**, *36*, 344−350.
(60) Jones, T. A.; Zou, J. Y.; Cowan S. W.; Kjeldgaard M. *Acta Crystallogr.* **1991**, *A47*, 11−19.

Table 3. X-ray Data for C42S Protein Crystals (Space Group *R*3)

	Fe^{III}	dithionite-treated
unit cell		
a	64.52	64.54
b	32.57	32.47
res limit, Å	1.65	1.7
no. of observations	40888	14658
no. of unique reflects	6061	5426
completeness, %	99.6	98.5
$R(I)_{merge}$[a] overall, %	6.8	4.5
$R(I)_{merge}$[a] highest res,%	14.1	15.1
no. of reflects used	5925	5407
R-factor,[b] %	18.5	16.8
R-free,[c] %	21.7	20.1
no. of solvent waters	48	51
mean *B* factor, Å^2	25.2	21.7
rms deviation from ideal values		
bond, Å	0.02	0.03
angle, deg	1.9	1.3
no. of residues in core regions[d]	92.7	91.7
no. of residues in allowed regions[d]	7.3	8.3

[a] $R = \sum||I_o| - |I_c||/\sum|I_o|$. [b] $R = \sum||F_o| - |F_c||/\sum|F_o|$. [c] Based on a subset of 5% of the reflections. [d] As output from the PROCHECK program.

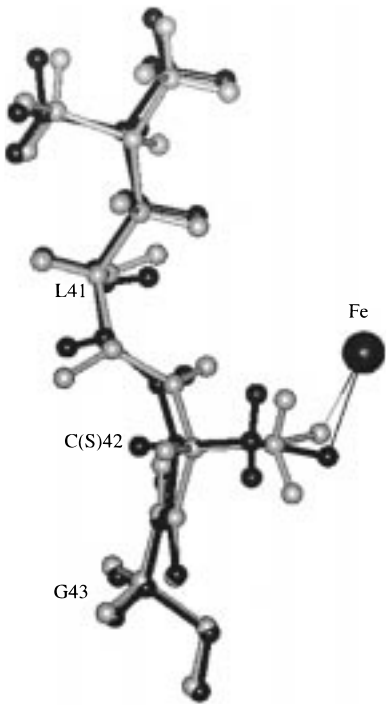

Figure 3. Overlay of ball-and-stick models of the Fe^{III}-C42S (light) and *Cp* rRd (dark) structures in the region of residue 42.

Fe^{III}-C42S Rubredoxin. The initial difference Fourier electron-density map displayed two main features. A 9σ negative peak at the position of C42-S$^\gamma$ and a pair of positive and negative peaks on either side of the iron atom were apparent, indicating the mutation of residue 42 and a movement of the iron atom toward C42-S$^\gamma$, respectively. Residue C42 was mutated to a serine using the program O. The cysteinyl sulfur atom was replaced with an oxygen atom (S42-O$^\gamma$) in the coordinate file. Figure 3 shows an overlay of structural models of the C42S protein and *Cp* rRd in the vicinity of residue 42.

Dithionite-Treated C42S Rubredoxin. The conventional *R*-value based on structure factor amplitudes between observations from the dithionite-treated form and calculated structure factors from the refined Fe^{III}-C42S model observed data was 31%, indicating significant structural differences between the two structures. A difference electron-density map with coefficients $|F_o| - |F_c|$, where the F_o values were observed structure amplitudes from the dithionite-treated structure and the F_c values were calculated from the Fe^{III}-C42S structure, revealed

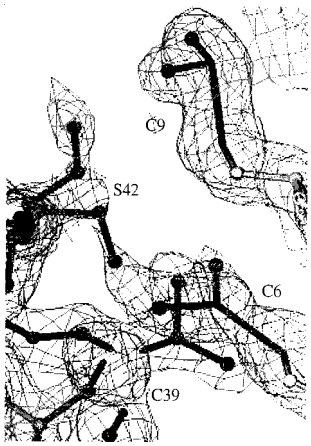

Figure 4. Model of the active site structure of the dithionite-treated Fe^{III}-C42S mutant of *Cp* Rd, superimposed on the final $2F_o - F_c$ difference map.

large areas of both positive and negative density in and around the active site. Electron-density difference omit maps, omitting the cysteine ligands from the calculated structure factors, were used to clarify the structure around the active site. The interior cysteines, C6 and C39, were present in conformations similar to those in *Cp* rRd and the C42S mutant. Surface residue C9 was found to fit the electron density in a conformation pointing away from the active site. A large crescent-shaped volume of electron density associated with C9 was modeled by the inclusion of an SO_2 group covalently bound to C9-S^γ. Two conformations for S42 were observed and modeled assuming 50% occupancy for each. A crescent-shaped volume of electron density was also observed in the position occupied by the iron atom in the oxidized structure. Attempts to place an iron atom in this position failed. The associated temperature factor refined to an unacceptably high value ($\sim$50 Å^2 compared with 20.8 Å^2 for the Fe atom in the oxidized structure). In fact, it was not possible to place an iron atom bonded to both C6-S^γ and C39-S^γ ligand atoms with acceptable geometry anywhere in the remaining electron density. It was clear that C6-S^γ only could be bound to the active site electron density. The most reasonable model which accounted for the observed shape of the electron density in this region involved inclusion of a second SO_2 unit bound covalently to C6-S^γ. Refinement of this model resulted in *B*-factors of about 17 Å^2 up to the S^γ atom and about 31 Å^2 further along the side chain. It is not possible to simultaneously accommodate one of the two conformations of S42 and the SO_2 unit on C6. The final model is consistent with a partially occupied SO_2 unit on C6 present only when S42 is in its more distant conformer. Figure 4 shows the active site structure of the final model, together with the final $2F_o - F_c$ electron-density map.

X-ray Absorption Spectroscopy. Measurements were carried out at the Stanford Synchrotron Radiation Laboratory with the SPEAR storage ring containing 55−90 mA at 3.0 GeV. Spectra were collected on beamline 7-3 using a Si(220) double crystal monochromator, with an upstream vertical aperture of 1 mm and a wiggler field on 1.8 T. Harmonic rejection was accomplished by detuning one monochromator crystal to approximately 50% off-peak, and no specular optics were present in the beamline. The incident X-ray intensity was monitored using a nitrogen-filled ionization chamber, and X-ray absorption was measured as the X-ray Fe Kα fluorescence excitation spectrum using an array of 13 germanium intrinsic detectors.[61] During data collection, samples were maintained at a temperature of approximately 11 K, using an Oxford Instruments liquid helium flow cryostat. Spectra at the Fe K-edge were calibrated with reference to the lowest energy inflection point of iron metal (assumed to be 7111.3 eV). The data were analyzed using the EXAFSPAK suite of computer programs.[62] The extended X-ray absorption fine structure (EXAFS) oscillations $\chi(k)$ were quantitatively analyzed by curve-fitting. The EXAFS total amplitude and phase-shift functions were calculated using the program *feff* (version 6.01).[63,64] Protein samples (7−10 mM) were prepared in buffer (100 mM) and NaCl (300 mM) at pH 4.0 (acetic acid), 6.0 (MES), and 8.0 (tricine). The samples were mixed with glycerol (30 vol %) as glassing agent before loading into Lucite sample cells fitted with Mylar tape windows. The samples were in the oxidized form as prepared. For reduced samples, dithionite solution (200 mM; 2−3 equiv) was added. The samples were frozen in liquid nitrogen immediately after preparation.

(61) Cramer, S. P.; Tench, O.; Yocum, M.; George, G. N. *Nucl. Instrum. Methods* **1988**, *A266*, 586−591.

(62) The EXAFSPAK program suite is available from http://ssrl01.slac.stanford.edu/exafspak.html.

Results

Characterization of Mutant Proteins. *Cp* Rd has been expressed in *E. coli* as a mixture of the Fe^{III} and Zn^{II} forms of the unformylated recombinant protein.[8,10,12] For mutant proteins, the relative content of Fe^{III} and Zn^{II} varies from case to case. Mutants C6S, C9S, C39S, and C42S each expressed as the Zn^{II} protein. However, it is possible in the present system to incorporate iron at the crude lysate stage of protein isolation by mild denaturation under reducing conditions followed by renaturation in the presence of excess Fe^{II}. Aerial oxidation of Fe^{II}-Rd produces stable Fe^{III} forms. Stable Cd^{II} forms of each of the present mutants have also been produced for NMR examination. However, attempts to incorporate Co^{II} into these mutant apo proteins were unsuccessful. Mixtures of apo and unstable Co^{II}-Rd forms were obtained although Co^{II} has been incorporated successfully into recombinant wild type protein.[65,66]

The identification of these proteins was confirmed by N-terminal sequencing for C6S and C9S and by electrospray ionization mass spectrometry (Figure 2 and Table 2). The mass spectrometry reveals a single peak at 6100(1) and 6084(1) Da, respectively, for *Cp* rRd and for its four cysteine to serine mutants, consistent with a sulfur atom being replaced by an oxygen atom in each mutant molecule. All four mutants, particularly C6S and C39S, are less stable than *Cp* rRd. For example, in 10% trichloroacetic acid, the mutant proteins decolor and precipitate completely in less than 5 min compared to at least 1 h for the native and recombinant forms.

Electronic spectra of the recombinant wild type protein and the four cysteine to serine variants are shown in Figure 5, and detailed absorption bands listed in Table 4. The spectrum of *Cp* rRd displays features at 350, 380, 490, 570, and 750 nm, arising from S → Fe^{III} charge-transfer transitions.[67,68] These bands are all shifted to higher energy upon replacement of a cysteinyl ligand by serine, leading to a change in protein color from red to orange. The band at 280 nm diminishes in intensity upon mutation, attributable to a decreased S → Fe^{III} charge-transfer contribution. Comparison of the spectra of the four mutants shows that those of the pairs C6S, C39S and C9S, C42S differ but are similar within each pair, consistent with the different environments of the interior (C6,39) and surface (C9,-42) ligands.

(63) Rehr, J. J.; Mustre de Leon, J.; Zabinsky, S. I.; Albers, R. C. *J. Am. Chem. Soc.* **1991**,*113*, 5135−5140.

(64) Mustre de Leon, J.; Rehr, J. J.; Zabinsky, S. I.; Albers, R. C. *Phys. Rev.* **1991**, *B44*, 4146−4156.

(65) The Co^{II} forms of interior ligand mutants C6S and C39S appeared to be more stable than those of surface ligand mutants C9S and C42S. Elution of the reconstitution mixture on a DE-52 anion exchange column resulted initially in a single protein band of Co^{II}-C6S but two bands for C9S. The pale green solution of Co^{II} proteins decolored gradually during storage. ESI-MS experiments suggested apo proteins as major products.

(66) Lucarelli, M. Honours Thesis, University of Melbourne, 1996.

(67) Lovenberg, W.; Sobel, B. E. *Proc. Natl. Acad. Sci. U.S.A.* **1965**, *54*, 193−199.

(68) Gebhard, M. S.; Deaton, J. C.; Koch, S. A.; Millar, M.; Solomon, E. I. *J. Am. Chem. Soc.* **1990**, *112*, 2, 2217−2231.

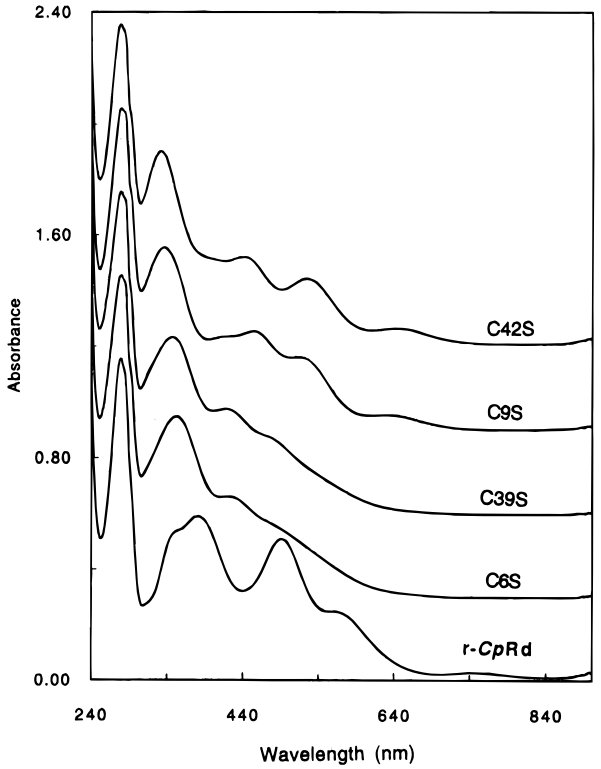

Figure 5. Electronic absorption spectra of oxidized *Cp* Rd proteins (0.13 mM in 50 mM Tris−HCl (pH, 7.4)). The spectra have been offset by 0.3 absorption unit for clarity.

Table 4. Electronic Absorption Spectra in 50 mM Tris−HCl (pH 7.5)[a]

protein	λ_{max}, nm (ϵ, 10^3 M^{-1} cm^{-1})
Cp rRd	750 (0.34), 570 (3.18, sh.), 490 (6.64), 380 (7.71), 350 (7.00, sh), 280 (15.0)
C6S	475 (3.35, sh), 420 (4.53), 350 (8.06), 280 (14.4)
C9S	630 (0.65), 512 (3.18, sh), 453 (4.31), 420 (4.08, sh), 335 (8.00), 280 (14.1)
C39S	475 (3.45, sh), 418 (4.69), 348 (7.92), 280 (14.4)
C42S	645 (0.81), 525 (3.08), 440 (4.06), 331 (8.91), 280 (14.6)

[a] Molar extinction coefficients of the recombinant protein were determined by quantitative drying of a sample of known absorbance in volatile ammonium bicarbonate buffer.

Resonance Raman spectra of recombinant protein and each cysteine to serine mutant are shown in Figure 6. Data are listed in Table 5. The spectrum of *Cp* rRd is identical to that of the native protein but differs significantly from that of each mutant, as expected for the substitution of an FeS_4 center by an $FeOS_3$ center. Again, the similarity in individual behavior of the interior (C6S, C39S) and surface (C9S, C42S) pairs of mutants is observed in the spectra (Figure 6), reflecting the pseudo-2-fold symmetry of the FeS_4 center in the native protein. The spectra remain to be analyzed in detail.

The EPR spectrum of *Cp* rRd at 4.2 K displays a resonance at $g = 9.32$ associated with one principal direction of the lowest Kramers doublet ($\pm 1/2$ or $\pm 5/2$) and a number of features in the $g = 4.0-4.8$ range associated with the three principal directions of the $\pm 3/2$ doublet.[69,70] Similar features are present in the EPR spectra of each of the mutant proteins (Table 6; Figure 7). Temperature dependencies of the spectra are similar to those of the native protein. The low-field resonance is shifted

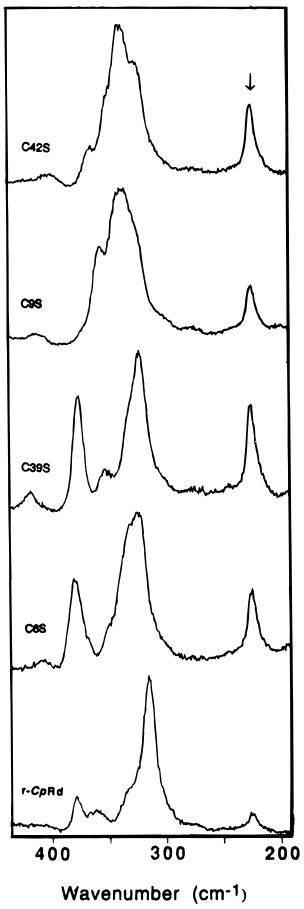

Figure 6. Resonance Raman spectra of oxidized *Cp* Rd proteins (50 mM Tris−Cl (pH, 7.4)) at 93 K obtained with 476.5 nm excitation (100 mW) and 2.7 cm^{-1} slit widths. The ice band at 225 cm^{-1} is indicated by an arrow.

Table 5. Resonance Raman Data in the Range of 250−400 cm^{-1} ($\lambda_o = 476.5$ nm)

protein		protein	
Cp rRd	316, ∼332 (sh), ∼362, 379	C39S	324, ∼354, 377
C6S	326, ∼332 (sh), ∼349 (sh), 380	C42S	328, 341, ∼356 (sh), 367
C9S	∼330 (sh), 339, 358		

Table 6. EPR Parameters for *Cp* Rd Proteins

protein	g_1	g_2	ref	protein	g_1	g_2	ref
Cp rRd	4.27	9.32		C9S	4.27	9.49	
	4.27	9.47	11	C39S	4.26	9.33	
	4.31	9.42	69	C42S	4.27	9.52	
C6S	4.26	8.98			4.27	9.65	11

significantly (g, 8.98), and all features are broader in the C6S mutant (Figure 7). This may reflect heterogeneity at the site in this case. The features are more complex for the C42S mutant.[11] The spectrum does not change upon dissolution of freeze-dried protein in ^2H_2O, and so the structure is not due to dissociable protons. The spectra of the other mutants also do not change upon deuteration.

Electrochemistry. Estimates of the reduction potentials of native and recombinant *Cp* Rd and mutants of *Cp* Rd by square wave voltammetry have employed a poly(L-lysine)-modified pyrolytic graphite edge electrode.[10,43] For the present mutants, only weak and unstable electrochemical responses were observed under the same conditions, presumably due to their decreased stability to denaturation and consequent blockage of

(69) Peisach, J.; Blumberg, W. E.; Lode, E. T.; Coon, M. J. *J. Biol. Chem.* **1971**, *246*, 5877−5881.
(70) Hagen, W. R. *Adv. Inorg. Chem.* **1992**, *38*, 165−222.

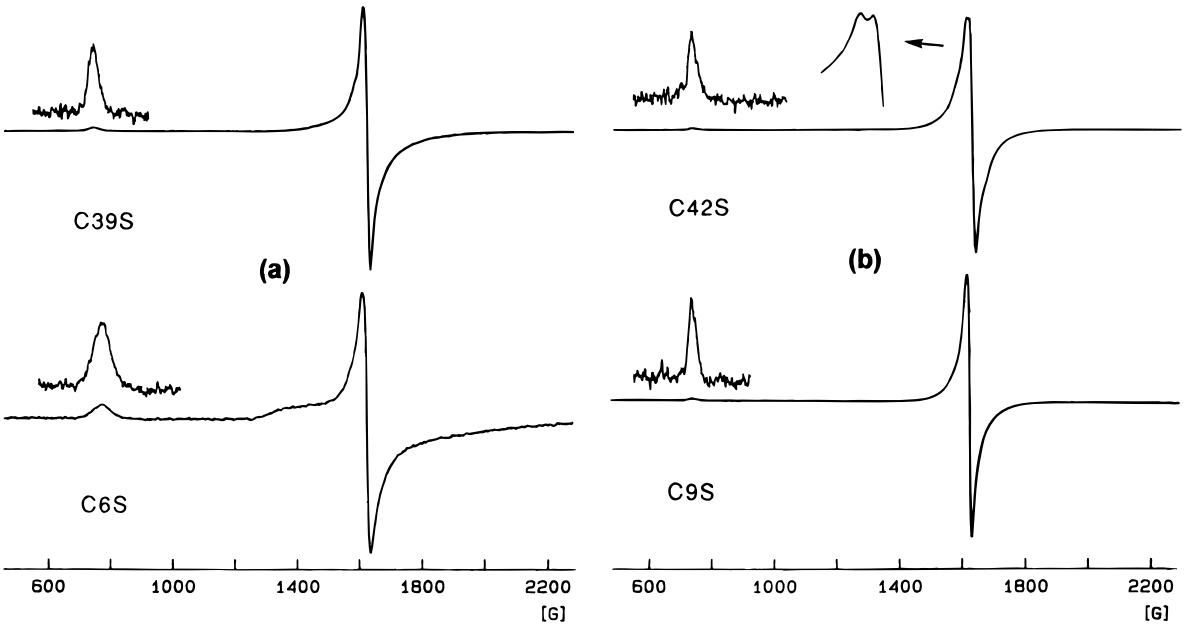

Figure 7. EPR spectra of oxidized *Cp* Rd proteins (1.6 mM in 50 mM Tris−HCl (pH 7.4) and 150 mM NaCl) at 4.2 K: (a) interior mutants; (b) surface mutants.

the active sites of the electrode surface by adsorbed protein. This difficulty can be alleviated by the addition of 1 equiv of poly(L-lysine) to the solution. The potential shifts positively due to the presence of poly(L-lysine) in the solution, but the magnitude of that shift can be estimated from the dependence of $E_{1/2}$ of *Cp* rRd on the molar ratio of poly(L-lysine) to the protein.[43] Steady, reversible electrochemistry was observed for surface ligand mutants C9S and C42S in the pH range 6−10: the peak potentials remained constant at different pulse frequencies, and a plot of the peak currents versus the square roots of those frequencies is linear (Figure 8). This is a one-electron couple, Fe^{III}/Fe^{II}, as characterized by the observed peak width at half-height of 127 ± 1 mV.[41] For the interior ligand mutant C6S, the observation of a similar reversible electrochemical response was limited to a pH range of 7.6−10.5. It was critically dependent on protein purity and on the condition of the electrode surface. Only highly purified protein and a freshly polished electrode produced a reversible electrochemical response (Figure 8). However, under the same conditions, C39S produced a weak and unstable electrochemical response only.

The reduction potential of native *Cp* Rd is pH-independent, as is that of *Cp* rRd.[71] Those of the Cys to Ser mutants do depend on pH (Figure 9). The electrochemistry of the surface ligand mutants, C9S and C42S, is chemically reversible in the range 10 > pH > 6 but becomes irreversible in the range 6 > pH > 5. This will not affect the estimation of peak potentials significantly as the subsequent chemical reactions are slow on the voltammetric time scale. The response disappears below pH 5. For the interior ligand mutant C6S, the response is chemically reversible in the range 10.5 > pH > 7.6 and disappears at pH 6.2.

Possible processes involving Fe^{III}/Fe^{II} couples may be depicted by Scheme 1.[72] Equation 1 may be derived for $T =$

$$E_{1/2} = E^{\circ}_{A} + 59 \log \frac{K_a^{ox}(K_a^{red} + [H^+])}{K_a^{red}(K_a^{ox} + [H^+])} \qquad (1)$$

298 K,[73,74] where $E_{1/2}$ is the observed midpoint potential (mV), E°_{A} the standard reduction potential for the deprotonated couple

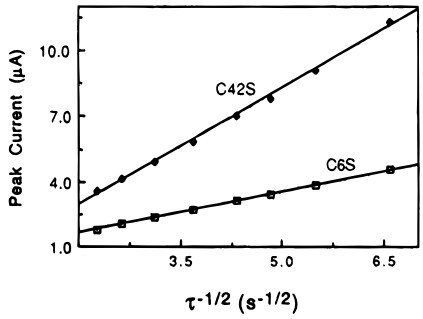

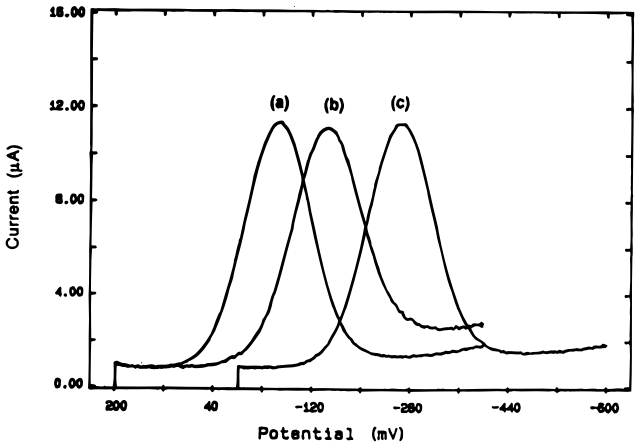

Figure 8. Square wave voltammograms of *Cp* Rd proteins (0.10 mM in 30 mM CHES (pH, 8.9) and 0.1 M NaCl): (a) recombinant; (b) C6S; (c) C42S. The peak current for the C6S protein is only about half that of C42S (see inset) but is adjusted to similar intensity for easy comparison. Conditions: $E_p = 50$ mV, $E_s = 1$ mV, $\tau^{-1} = 30$ Hz. Inset: plots of peak current I_p versus the square root of the frequency of the applied potential pulse $\tau^{-1/2}$.

(Fe^{III}/Fe^{II}, in this case) and K_a^{ox} and K_a^{red} are the proton dissociation constants of the oxidized and reduced forms, respectively.

(71) Im, S.-C.; Zhuang-Jackson, H.-U.; Kohzuma, T.; Kyritsis, P.; McFarlane, W.; Sykes, A. G. *J. Chem. Soc., Dalton Trans.* **1996**, 4287−4294.

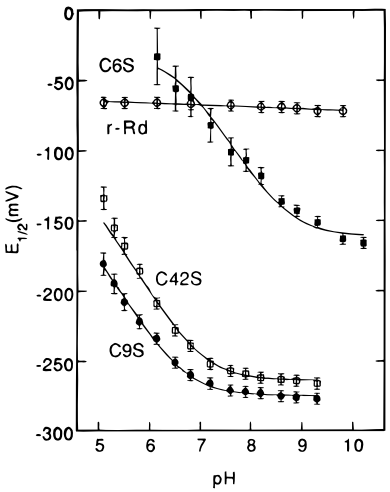

Figure 9. Variation of $E_{1/2}$ with pH for *Cp* rRd and C to S mutant proteins. The lines are fittings of eq 1 to the experimental data. Conditions are as in Figure 8.

Scheme 1

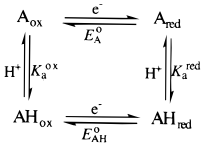

Table 7. Square Wave Voltammetry Data at 25 °C[a]

protein	E°_{A}, mV	pK_a^{red}	pK_a^{ox}	protein	E°_{A}, mV	pK_a^{red}	pK_a^{ox}
rRd	−77			C9S	−284	6.7	<4
C6S	−170	8.7	<6	C42S	−273	7.0	<4
C39S	∼ −190						

[a] Parameters derived by curve fitting of the experimental data to eq 1 (Figure 9) and corrected for the shift induced by the poly-L-lysine promoter (see ref 43).

Fitting of eq 1 to the data provides estimates of parameters E°_{A}, K_a^{red}, and K_a^{ox} (Table 7; Figure 9). Large errors are associated with the estimates of K_a^{ox} due to lack of experimental data at lower pH.

Molecular Structure of Fe^{III}-C42S Rubredoxin. The observation of a S42 O$^{\gamma}$−Fe distance of 1.82(8) Å confirms the presence of an $FeOS_3$ center (Table 8; Figure 3). Synthetic $[Fe^{III}(OAr)_4]^-$ complexes featuring substituted phenoxy ligands OAr exhibit Fe−O distances of 1.83−1.87 Å.[75] The S42-O$^{\gamma}$−Fe and -O$^{\gamma}$−C$^{\beta}$ distances are 0.4 Å shorter than the equivalent distances to C42-S$^{\gamma}$ in *Cp* rRd.[76] In turn, this imposes increases of 22° and 8° in the S42-C$^{\beta}$−O$^{\gamma}$−Fe and C6-S$^{\gamma}$−Fe−O$^{\gamma}$-S42 angles, respectively, and 12° in the S42-C$^{\alpha}$−C$^{\beta}$−O$^{\gamma}$−Fe dihedral angle. The data are consistent with the generally larger value of the M−O−C bond angle (range, 110−140°) in olate complexes relative to the M−S−C angle (range, 100−120°) in thiolate complexes.[14]

The polypeptide chain carrying interior ligands C6 and C39 is constrained by the rigid aromatic core of the protein.[5] The sections carrying surface ligands C9 and C42 will have greater conformational flexibility. When combined with the electronic and steric implications of substitution of ligand atom S by O, these features appear to be responsible for the observed structural variations (Table 8). In particular, major structural changes are limited to the region of the mutation: the polypeptide chain "kinks", with the C$^{\alpha}$ and C$^{\beta}$ atoms of residue 42 moving 0.4(1) and 0.5(1) Å, respectively, toward the iron atom (Figure 3). Closer packing of atoms is apparent in this local surface region. For example, the separation of H$^{\beta 2}$ atoms on residues 9 and 42 (cf. Figure 1) is 2.3 Å in *Cp* rRd but less than 2 Å in C42S (assuming r(C−H) = 1.09 Å; the H···H van der Waals separation is about 2.4 Å[77]).

Table 8. Comparison of Coordination Spheres in Fe^{III}-*Cp* Rd and Its C42S Mutant

	rRd[a]	C42S[b]	Δ[c]
Bond Distances, Å			
6S$^{\gamma}$−Fe	2.29	2.32	0
9S$^{\gamma}$−Fe	2.25	2.37	+0.1
39S$^{\gamma}$−Fe	2.28	2.36	+0.1
42(S$^{\gamma}$,O$^{\gamma}$)−Fe	2.23	1.82	−0.4
6S$^{\gamma}$−C$^{\beta}$	1.79	1.78	0
9S$^{\gamma}$−C$^{\beta}$	1.86	1.83	0
39S$^{\gamma}$−C$^{\beta}$	1.81	1.82	0
42(S$^{\gamma}$,O$^{\gamma}$)−C$^{\beta}$	1.82	1.41	−0.4
mean esd	<0.01[a]	0.08	0.1
Bond Angles, deg			
6S$^{\gamma}$−Fe−9S$^{\gamma}$	113.4	113	0
6S$^{\gamma}$−Fe−39S$^{\gamma}$	110.1	110	0
6S$^{\gamma}$−Fe−42(S$^{\gamma}$,O$^{\gamma}$)	104.3	112	+8
9S$^{\gamma}$−Fe−39S$^{\gamma}$	104.6	101	−4
9S$^{\gamma}$−Fe−42(S$^{\gamma}$,O$^{\gamma}$)	112.7	113	0
39S$^{\gamma}$−Fe−42(S$^{\gamma}$,O$^{\gamma}$)	111.9	108	−4
42C$^{\beta}$−(S$^{\gamma}$,O$^{\gamma}$)−Fe	110.2	132	+22
mean esd	0.1	3	3
Dihedral Angles, deg			
6C$^{\alpha}$−C$^{\beta}$−S$^{\gamma}$−Fe	169.7	166	−4
9C$^{\alpha}$−C$^{\beta}$−S$^{\gamma}$−Fe	93.8	100	+6
39C$^{\alpha}$−C$^{\beta}$−S$^{\gamma}$−Fe	175.8	170	−6
42C$^{\alpha}$−C$^{\beta}$−(S$^{\gamma}$,O$^{\gamma}$)−Fe	88.1	100	+12
Hydrogen Bond Distances, Å			
6S$^{\gamma}$···N8	3.68	3.70	0
6S$^{\gamma}$···N9	3.65	3.71	+0.1
9S$^{\gamma}$···N11	3.49	3.42	−0.1
39S$^{\gamma}$···N41	3.54	3.54	0
39S$^{\gamma}$···N42	3.58	3.56	0
42(S$^{\gamma}$,O$^{\gamma}$)···N44	3.84	4.00	+0.2

[a] Taken from ref 76. Esds are 0.003 Å: distances are quoted to three figures only to allow convenient comparison with distances in C42S. [b] Present work. [c] A positive value means an increase in C42S relative to rRd.

Six S···N distances in the range 3.5−3.9 Å separate cysteine S$^{\gamma}$ and peptide HN functions around the active site in *Cp* rRd (Figure 1; Table 8). The S···N separation for typical S···HN hydrogen bonds is around 3.4 Å.[78] In particular, the C42-S$^{\gamma}$···HN-V44 interaction (3.844(3) Å[79]) has been described as weak or "incipient".[79] Within experimental error, the S···N distances are the same in the C42S protein. The S42-O$^{\gamma}$···N-V44 distance is 4.0 Å which can be compared with an expected O···N separation of 2.8 Å for a typical O···HN hydrogen bond.[78] It is apparent that a S42-O$^{\gamma}$···HN-V44 hydrogen bond is not present in the C42S protein.

Molecular Structure of Dithionite-Treated C42S Rubredoxin. A crystal of the Fe^{III}-C42S mutant protein was treated

(72) Clark, W. M. *Oxidation−Reduction Potentials of Organic Systems*; Williams & Wilkins: Baltimore, 1960.

(73) Dutton, P. L. *Methods Enzymol.* **1978**, *54*, 411.

(74) $E_{1/2} = E^{\circ}_{AH} + 59 \log (K_a^{red} + [H^+])/(K_a^{ox} + [H^+])$, where E°_{AH} is the standard reduction potential for the protonated couple, is equivalent to eq 1.

(75) Koch, S. A.; Millar, M. *J. Am. Chem. Soc.* **1982**, *104*, 5255−5257.

(76) Dauter, Z.; Wilson, K. S.; Sieker, L. C.; Moulis, J.-M.; Meyer J. *Proc. Natl. Acad. Sci. U.S.A.* **1996**, *93*, 8836−8840.

(77) Huhey, J. E.; Keiter, E. A.; Keiter, R. L. *Inorganic Chemistry*, 4th ed.; Harper- Collins: New York, 1993; p 292.

(78) Hamilton, W. C.; Ibers, J. A. *Hydrogen Bonding in Solids;* Benjamin: New York, 1968; p 16.

(79) Adman, E.; Watenpaugh, K. D.; Jensen, L. H. *Proc. Natl. Acad. U.S.A.* **1975**, *72*, 4854−4858.

Table 9. Structural Parameters for C−S−SO_2 Fragments in Dithionite-Treated C42S *Cp* rRd and Metal Complexes

	C6[a]	C9[a]	Ru^{II} [b]	Cu^{I} [c]
Bond Distances, Å				
$S^{\gamma}-C^{\beta}$	1.8	1.8	1.79	1.76
$S^{\gamma}-S^{\delta}$	2.5	2.4	2.84	2.53
$S^{\delta}-O^{\epsilon 1}$	1.5	1.5	1.32	(1.44)[d]
$S^{\delta}-O^{\epsilon 2}$	1.5	1.5	1.42	(1.44)[d]
mean esd	0.1	0.1	0.01	0.01
Bond Angles, deg				
$C^{\alpha}-C^{\beta}-S^{\gamma}$	112	116		
$C^{\beta}-S^{\gamma}-S^{\delta}$	85	102	97	95
$S^{\gamma}-S^{\delta}-O^{\epsilon 1}$	138	92	95	106
$S^{\gamma}-S^{\delta}-O^{\epsilon 2}$	84	103	103	110
$O^{\epsilon 1}-S^{\delta}-O^{\epsilon 2}$	97	111	112	(114)[d]
mean esd	5	5	1	1
Dihedral Angles, deg				
$C^{\alpha}-C^{\beta}-S^{\gamma}-S^{\delta}$	158	97	131, 128[e]	109, 148[e]
$C^{\beta}-S^{\gamma}-S^{\delta}-O^{\epsilon 1}$	102	59	82	84
$C^{\beta}-S^{\gamma}-S^{\delta}-O^{\epsilon 2}$	165	172	148	140
angle ω[f]	41	14	17	35

[a] This work. [b] (η^5-C_5H_5)(PPh_3)(SO_2)Ru^{II}{S(SO_2)-4-C_6H_4Me} (ref 82). [c] (PPh_2Me)$_3Cu^{I}${S(SO_2)-Ph} (ref 83). [d] The SO_2 unit was refined as a rigid body of constrained geometry. [e] There are two angles as there are two ortho carbons in the aromatic rings of these fragments. [f] Angle between the S−S vector and SO_2 plane.

with dithionite at pH 4 in an attempt to produce the reduced Fe^{II}-C42S form. However, the current structural model indicates that the iron atom is missing. SO_2, the oxidized form of the reducing agent SO_2^-, is bound to C9, forming a $[CH_2S^{\gamma}S^{\delta}O^{\epsilon}{}_2]^-$ side chain which defines part of the protein surface (Figure 4). About half of the molecules in the crystal feature another SO_2 bonded to C6-S^{γ}. This second $[CH_2SSO_2]^-$ unit is located in the space occupied by the iron atom in *Cp* Rd.

S42 is present in two conformations, one directed toward the C6 fragment and one directed away (Figure 4). It is probable that molecules with the former arrangement do not possess the C6-SSO_2^- unit as the $O^{\gamma}\cdots O^{\epsilon}$ separation between S42-O^{γ} and C6-$S^{\gamma}S^{\delta}O^{\epsilon}{}_2^-$ fragments would be unacceptably short (about 2 Å; typical hydrogen-bonding separation, 2.7 Å[78]). This suggestion is consistent with the temperature factor associated with the C6-S^{δ} atom being twice that of C6-S^{γ}, indicating that the occupancy of C6-S^{δ} is about half that of C6-S^{γ}. In addition, products containing one and two SO_2 units were isolated in solution phase experiments at pH 4 (vide infra; Table 2).

The structural parameters of the proposed CH_2-$S^{II}-S^{IV}O_2^-$ side chains are listed in Table 9. The S−S distances, 2.5(1) and 2.4(1) Å, are much shorter than the sum of the van der Waals radii, 3.6 Å,[77] but longer than the distance of a typical S−S single bond, 2.0−2.15 Å.[80] They are similar to that, 2.39 Å, seen for the dithionite ion in $Na_2S_2O_4{\cdot}2H_2O$.[81] The bond and dihedral angles indicate a pyramidal geometry around the S^{δ} atoms (Table 9), consistent with the presence of a stereochemically active lone pair of electrons characteristic of oxidation state IV. Such fragments have been observed previously as ligands bound to metal atoms via the S^{II} atom in complexes (η^5-C_5H_5)(PPh_3)(SO_2)Ru^{II}{S(SO_2)-4-C_6H_4Me} and (PPh_2Me)$_3Cu^{I}${S(SO_2)-Ph}, produced via reaction of metal−thiolate precursors with SO_2.[82,83] Relevant structural parameters are included in Table 9 for comparison. The significant variation in the bond lengths and dihedral angles estimated for C6-SSO_2^- relative to those for C9-SSO_2^- and the complexes may be related to the steric interactions experienced by the C6 fragment in the "active site".

Support for the addition of SO_2 fragments to the protein is provided by experiments in which solutions of the C42S protein (6 mM; acetate buffer (100 mM)) were reduced by sodium dithionite (20 equiv) at pH 4. The orange solution bleached immediately. After isolation on a G25 gel filtration column in air (eluent, H_2O or ammonium acetate (10 mM)), the protein products were examined by electrospray ionization mass spectrometry (Table 2; Figures S1 and S2 in the Supporting Information). At least three series of peaks were detected under these oxidizing conditions. Their relative abundance varied considerably with the exact conditions. Each series is assignable to a number of metal-free apo protein species in which redox modifications to one or more of the three Cys residues has occurred. The first series comprises an oxidized form featuring one cystine disulfide link, apo(SS, SH), bound to 0, 1, and 2 Na^+ ions. A second series is assignable to apo(SS, SSO_2^-) (in which the third Cys residue binds a SO_2 fragment) bound to 0, 1, and 2 Na^+ ions. The third is consistent with an apo(SH, $2SSO_2^-$) form with one Cys-SH and two Cys-SSO_2^- fragments bound to 0 and 1 Na^+ ions.

X-ray Absorption Spectroscopy. For surface ligand mutants C9S and C42S, a pK_a^{red} of about 7 was estimated for the reduced form (Table 7). In addition to oxidized Fe^{III} forms, samples reduced by sodium dithionite were examined at pH 8, 6, and 4 in 30% glycerol. The reduced pH 8 and 6 samples could be recovered quantitatively in pure oxidized form after removal of dithionite and glycerol in air. However, apo forms only could be recovered from the reduced pH 4 samples, consistent with the mass spectral data presented above. For interior ligand mutants C6S and C39S, some decomposition (<10%) was observed at pH 8 and complete decomposition at pH 6.

X-ray absorption near-edge spectra for Fe^{III}- and Fe^{II}-*Cp* rRd at pH 8.0 were very similar to those, typical of tetrahedral coordination, observed for the equivalent forms of native *Cp* Rd, Rd*Pa* and Rd*Pf*.[84−88] The bond lengths of 2.27(1) and 2.33(1) Å for Fe^{III}−S and Fe^{II}−S, respectively, provided by the EXAFS curve fitting (Table 10) are within experimental error of those for Rd*Pa* and Rd*Pf*. The Fe^{III}−S distance can be compared with the value of 2.26(3) obtained by averaging the range of distances obtained by X-ray crystallography (Table 8).[76] A change of pH to 4, that used for the crystallization experiments, had no effect on the average Fe^{III}−S distances.

The near-edge spectra of the Fe^{III} forms of the four Cys to Ser mutants were also typical of pseudotetrahedral geometry (e.g., Figure 10). In contrast, the near-edge spectra of the Fe^{II} forms contained nontetrahedral features and, in particular, the peak on top of the edge at about 7123 eV. The intensity of this feature correlated approximately with the observed Fe−O bond lengths (Table 10), being most intense with Fe^{II}-C9S at pH 6 (data not shown). Assuming an $FeOS_3$ center, curve fitting of data for the Fe^{III}-C42S protein obtained at pH 4 (the crystallization pH) provided Fe^{III}−S and Fe^{III}−O distances of 2.29(1) and 1.84(1) Å (Figure 10, Table 10). The equivalent X-ray crystallographic estimates are 2.35(8) and 1.82(8) Å

(80) Cotton, F. A.; Wilkinson, G. *Advanced Inorganic Chemistry*, 5th Ed.; Wiley: New York, 1988; p 523.
(81) Dunitz, J. D. *Acta Crystallogr.* **1956**, *9*, 579−586.
(82) Shaver, A.; Plouffe, P.-Y. *Inorg. Chem.* **1992**, *31*, 1823−1826.
(83) Eller, P. G.; Kubas, G. J. *J. Am. Chem. Soc.* **1977**, *99*, 4346−4351.
(84) Shulman, R. G.; Eisenburger, P.; Blumberg, W. E.; Stombaugh, N. A. *Proc. Natl. Acad. U.S.A.* **1975**, *72*, 4003−4007.
(85) Sayers, D. E.; Stern, E. A.; Herriott, J. R. *J. Chem. Phys.* **1976**, *64*, 427−428.
(86) Bunker, B.; Stern, E. A. *Biophys. J.* **1977**, *19*, 253−264.
(87) Shulman, R. G.; Eisenburger, P.; Teo, B. K.; Kincaid, B. M.; Brown, G. S. *J. Mol. Biol.* **1978**, *124*, 305−321.
(88) George, G. N.; Pickering, I. J.; Prince, R. C.; Zhou, Z. H.; Adams, M. W. W. *J. Biol. Inorg. Chem.* **1996**, *1*, 226−230.

Table 10. EXAFS Curve Fitting Results[a]

protein	Fe oxid state	pH	Fe−S, Å	σ^2,[b] Å^2	Fe−O, Å	σ^2,[b] Å^2	$E°$,[c] eV	error[d]
rRd	III	8.0	2.274(1)	0.0019(1)			−8.8(7)	0.331
	III	4.0	2.274(1)	0.0018(1)			−8.8(7)	0.325
	II	8.0	2.332(2)	0.0026(2)			−9.3(7)	0.391
C6S	III	8.0	2.280(1)	0.0027(1)	1.869(5)	0.0024(5)	−8.8(7)	0.310
	II	8.0	2.323(2)	0.0029(2)	2.094(9)	0.002(1)	−9.3(7)	0.423
C9S	III	8.0	2.285(1)	0.0019(1)	1.843(4))	0.000(3)	−8.8(7)	0.334
	II	8.0	2.354(1)	0.0022(1)	1.921(8)	0.004(1)	−9.3(7)	0.374
	II	6.0	2.334(3)	0.0042(3)	2.110(6)	0.000(5)	−9.3(7)	0.457
C39S	III	8.0	2.281(2)	0.0027(2)	1.865(6)	0.0016(6)	−8.8(7)	0.399
	II	8.0	2.319(2)	0.0021(2)	2.064(6)	0.000(7)	−9.3(7)	0.457
C42S	III	8.0	2.290(1)	0.0013(1)	1.836(5)	0.0006(5)	−8.8(7)	0.379
	III	4.0	2.293(1)	0.0020(2)	1.832(5)	0.0004(5)	−8.8(7)	0.414
	II	8.0	2.357(2)	0.0027(2)	1.928(8)	0.003(1)	−9.3(7)	0.461
	II	6.0	2.324(2)	0.0024(2)	2.092(7)	0.0009(8)	−9.3(7)	0.374

[a] Values in parentheses are estimated standard deviations from the diagonal elements of the covariance matrix. These values are precisions, and the accuracies (generally larger) are difficult to estimate. For bond lengths, the commonly accepted upper limit is between ±0.001 and ±0.002 Å. [b] Debye−Waller factors. [c] Threshold energy shift. [d] Fit error defined as $\sum[(\chi_{obsd} - \chi_{calcd})^2k^6]/\sum[(\chi_{obsd}{}^2k^6]$.

(Table 8). No significant variation is seen at pH 8 (Table 10). Equivalent data for the oxidized C6S, C9S, and C39S proteins at pH 8 confirm the presence of an Fe^{III}−O bond in each. The Fe^{III}−O distances may be longer in the interior ligand mutants C6S and C39S (1.87(1) Å) than in the surface ligand mutants C9S and C42S (1.84(1) Å).

For the surface ligand mutants C9S and C42S, curve fitting indicates that Fe−O distances increase from 1.84(1) to 1.92(1) Å upon reduction of Fe^{III} to Fe^{II} at pH 8 (Figures 10, 11; Table 10), consistent with the larger radius of a ferrous ion. However, at pH 6, the increases are much larger, and data at pH 8 for the interior ligand mutants C6S and C39S match the behavior of the surface mutants at pH 6 (σ, 0.01 Å):

pH		8	8	6
Fe oxid state		III	II	II
surface ligand:	C9S	1.84	1.92	2.11
	C42S	1.84	1.93	2.09
interior ligand:	C6S	1.87	2.09	
	C39S	1.87	2.06	

These structural changes apparently reflect the different pK_a^{red} values of about 7 and 9 derived electrochemically for the surface and interior ligand mutant proteins, respectively (Figure 9).

Nuclear Magnetic Resonance. Effective substitution of diamagnetic Cd^{II} for paramagnetic Fe^{III} was confirmed for the recombinant and mutant proteins by mass spectrometry (Table 2). In addition, a single resonance was observed in ^{113}Cd NMR spectra (Table 11). Synthetic tetrahedral Cd^{II}−thiolate centers resonate in the range 600−750 ppm.[89,90] By comparison, a range of 684−751 ppm has been observed for mononuclear Cd-$(SR)_4$ centers in proteins, and *Cp* rRd falls in this range.[89−94] The ^{113}Cd resonances in the CtoS mutants are deshielded relative to the recombinant protein (729.4 ppm) and fall in the range 604−645 ppm. Mutation of a buried ligand (C6,39) gives a higher chemical shift than does mutation of a surface ligand (C9,42). This range can be compared with the 630−670 ppm spread observed for proteins proposed to feature Cys_3His sites (CdS_3N).[89,90,95−98]

Complete ^{1}H resonance assignments for ^{113}Cd-*Cp* rRd were made using established techniques.[99,100] The assignments are summarized in Table S1. They are consistent with those of Zn^{II}-*Cp* rRd, and the secondary structures are qualitatively similar.[12,101] Short-range NOEs are summarized in Figure S3. Comparison of ^{1}H NMR spectra of the ^{113}Cd-substituted forms of the four CtoS mutants with that of Cd-*Cp* rRd allowed identification of the serine H^α and H^β resonances. For spin systems which were broadened and/or shifted significantly, sequential NOE connectivities were used to confirm assignments.

Resolved ^{1}H−^{113}Cd coupling to the serine H^β nuclei was not detected in 2D experiments. However, {^{1}H−^{113}Cd} HMQC spectra for the surface ligand mutants C9S and C42S show that coupling through the oxygen is present to both β protons (Figure 12), establishing the presence of a Cd−O-Ser link in those proteins. Equivalent experiments for the interior ligand mutants C6S and C39S failed to identify such coupling unequivocally.

A TOCSY spectrum of the interior ligand C6S mutant exhibits four cross-peaks which correlate with S6-NH (8.42 ppm). One of these (5.55 ppm) is very weak (Figure 13a,c). The correlations are confirmed by a DQF-COSY experiment, where S6-$H^{\beta a,b}$ (2.98 and 3.80 ppm) resonances show scalar connectivity to both S6-H^α (4.25 ppm) and the resonance at 5.55 ppm (Figure 14). The latter is assigned to a S6-OH^γ proton. Further evidence comes from weak NOE interactions between S6-OH^γ and V8,C9-NH resonances (Figure 13c). In addition, V8-$H^{\gamma a,b}$ and V44-$H^{\gamma a}$ resonances demonstrate weak NOE connectivities with S6-OH^γ (Figure 13c,d). Each of these protons will be close to a S6-OH^γ proton (Figure 1).

Two-dimensional experiments acquired in D_2O for the surface

(89) Coleman, J. E. *Methods Enzymol.* **1993**, *227*, 16−43.
(90) Summers, M. F. *Coord. Chem. Rev.* **1988**, *86*, 43−134.
(91) Myers, L. C.; Terranova, M. P.; Ferentz, A. E.; Wagner, G.; Verdine, G. L. *Science* **1993**, *261*, 1164−1167.
(92) Zerbe, O.; Pountney. D. L.; von Philipsborn, W.; Vasak, M. *J. Am. Chem. Soc.* **1994**, *116*, 377−378.
(93) Blake, P. R.; Lee, B.; Summers, M. F.; Park, J.-B.; Zhou, Z. H.; Adams, M. W. W. *New J. Chem.* **1994**, *18*, 387−395.
(94) Rusnak, F.; Czaja, C.; Kakalis, L. T.; Armitage, I. M. *Inorg. Chem.* **1995**, *34*, 3833−3834.
(95) Fitzgerald, D. W.; Coleman, J. E. *Biochemistry* **1991**, *30*. 5195−5201.
(96) South, T. L.; Kim, B.; Summers, M. F. *J. Am. Chem. Soc.* **1989**, *111*, 395−396.
(97) Giedroc, D. P.; Johnson, B. A.; Armitage, I. M.; Coleman, J. E. *Biochemistry* **1989**, *28*, 2410−2418.
(98) Giedroc, D. P.; Qiu, H.; Khan, R.; King, G. C.; Chen, K, *Biochemistry* **1992**, *31*, 765−774.
(99) Wuthrich, K. *NMR of Proteins and Nucleic Acids*; Wiley-Interscience: New York, 1986.
(100) Wagner, G.; Zuiderweg, E. R. P. *Biochem. Biophys. Res. Commun.* **1983**, *113*, 854−860.
(101) There are specific differences in the assignments of P15, N25, and D35. The present assignments are confirmed via sequential and long-range NOE interactions, and, in the case of P15, by observation of NOE interactions between N14-H^α and P15-H^δ and -$H^{\delta'}$ protons.

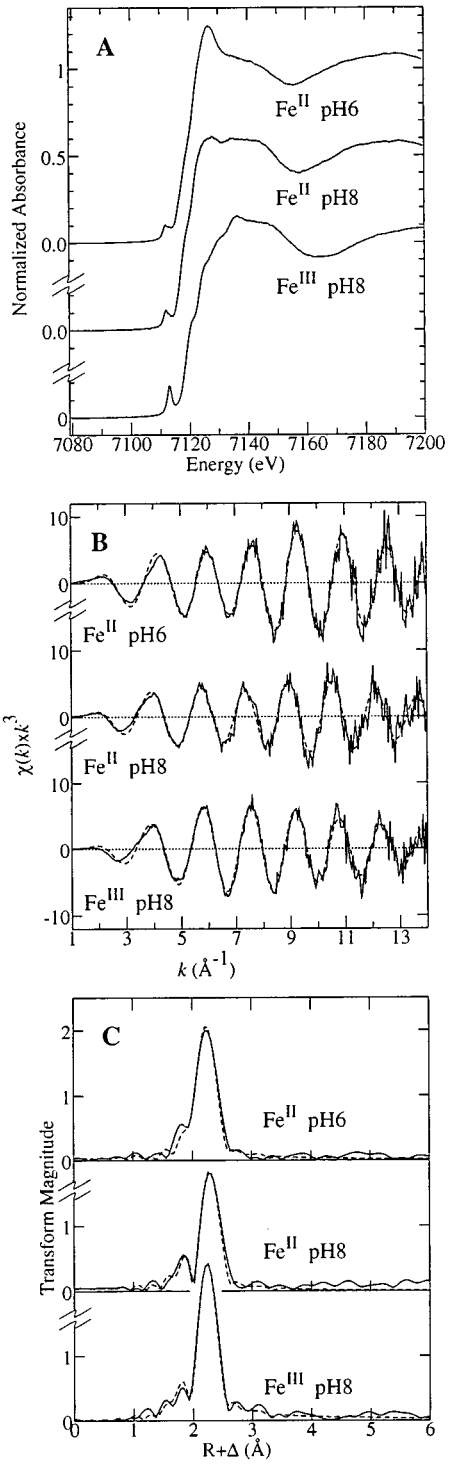

Figure 10. X-ray absorption spectroscopy of C42S-*Cp* rRd proteins: (A) near-edge X-ray absorption spectra; (B) k^3-weighted EXAFS data (experimental and best fit plots); (C) EXAFS Fourier transforms (phase-corrected for Fe−S back-scattering).

ligand mutant C42S demonstrate that the S42-H$^{\beta a,b}$ resonances are separated by only 0.03 ppm (4.10 and 4.13 ppm; Table 11). The V44-C$^{\gamma}$H$_3$ groups are within 3 Å of S42-O$^{\gamma}$ and -H$^{\beta}$ atoms in the crystal structure of the Fe^{III}-C42S mutant (cf. Figure 1). In D_2O, an unresolved NOE cross-peak is identified between V44-H$^{\gamma}$ and -H$^{\beta a,b}$ resonances while, in H_2O, a distinct NOE cross-peak is revealed between V44-H$^{\gamma}$ and a resonance at 4.07 ppm. A TOCSY spectrum acquired in H_2O shows that this additional resonance is correlated with the S42 spin system and consequently is assigned to S42-OH$^{\gamma}$.

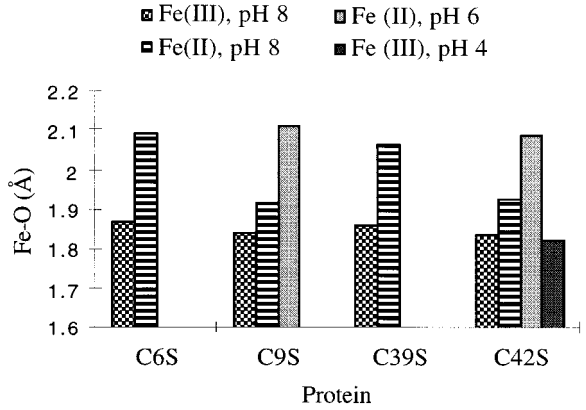

Figure 11. Fe−O distance comparisons in CtoS mutant rubredoxin proteins.

Table 11. ^{1}H and ^{113}Cd Chemical Shifts (ppm) for Mutant Proteins

		serine			
protein	Cd	H$^{\alpha}$	H$^{\beta}$	H$^{\gamma}$	NH
recomb	729.4				
C6S	626.3	4.25	2.98 3.80	5.55	8.42
C39S	644.8	*a*	*a*	*a*	*a*
C9S	614.8	4.81	4.08 4.28	*a*	8.82
C42S	604.7	4.87	4.10 4.13	4.07	8.95

[a] These resonances have not been identified unambiguously with the present data.

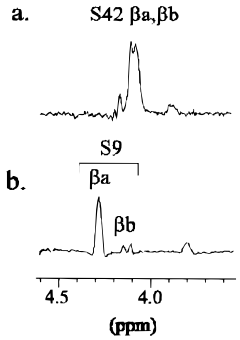

Figure 12. {^{1}H−^{113}Cd} HMQC spectra of (a) C42S (D_2O) and (b) C9S (H_2O) mutants. Evolution period optimized for 7 Hz coupling.

All backbone amide proton resonances in the C6S and C42S mutants are sharp. On the other hand, broadening is observed for protons close to the active sites in both C9S and C39S mutants. In the C9S mutant, broadening is restricted to the S9-NH resonance and that of Y11-NH, its type II NH···S donor to C9-S$^{\gamma}$ in the native form. The C39S mutant demonstrates significant broadening associated with residues close to the site of mutation (V38-G45). In fact, the present experiments could not detect resonances from residues S39 and C42. Consequently, the identification of Ser-OH$^{\gamma}$ resonances has not been possible for these two mutants.

The crystal structure of the C42S protein confirms the absence of a S42-O$^{\gamma}$···HN-V44 hydrogen bond in that mutant (O···N, 4.0 Å; Table 8). Thus, the O for S substitution eliminates the (incipient) hydrogen bond present in the native protein (Figure 1). A shift of 1.65 ppm upfield of the V44-NH resonance correlates with that loss (Table 12). In fact, in each C to S mutant protein, there is an upfield shift of 1.6−1.9 ppm for each NH proton that interacts with the relevant S$^{\gamma}$ atom in the

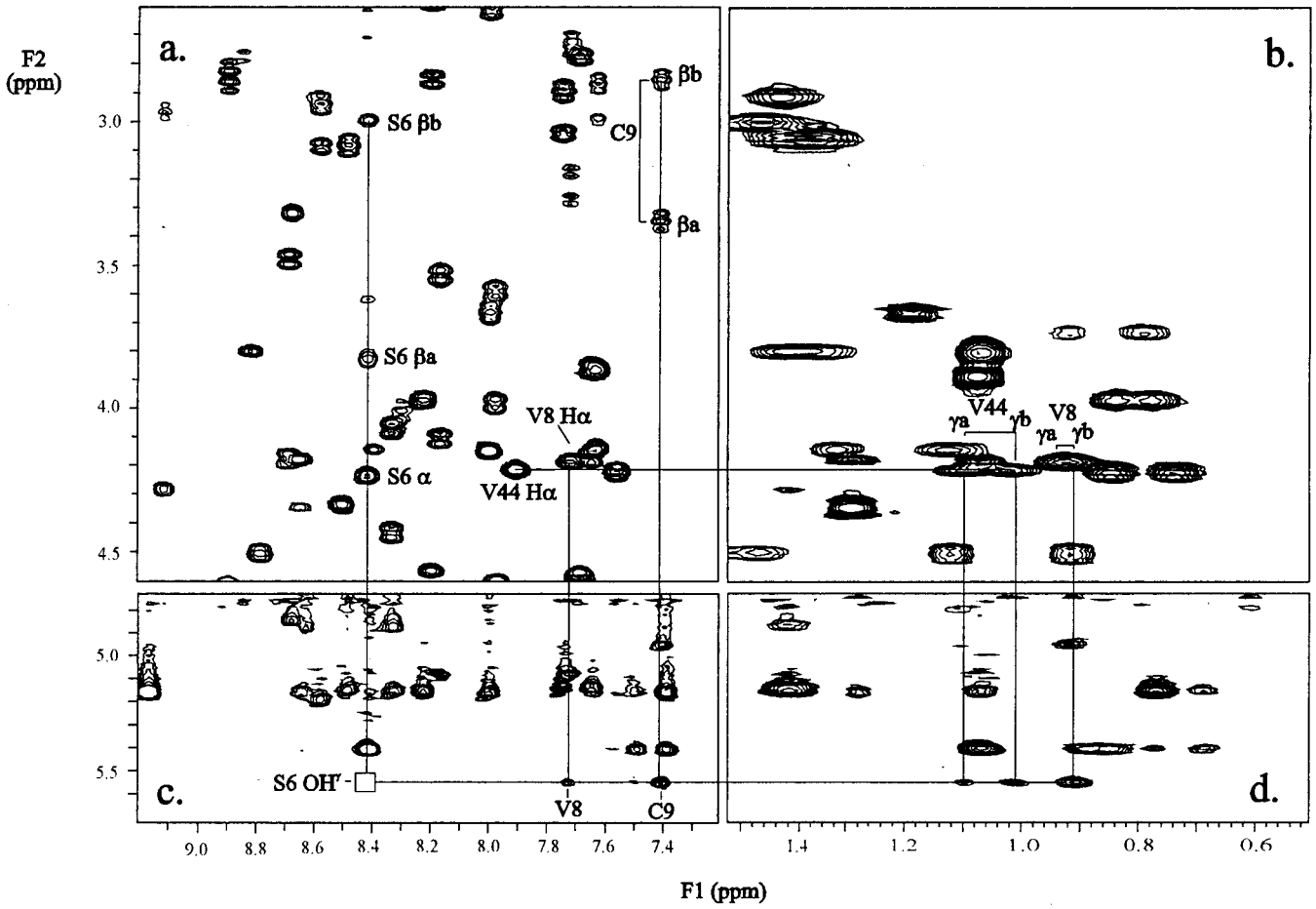

Figure 13. Identification of NOE connectivities with the S6 spin system in the C6S mutant. (a) and (b) are TOCSY spectra; NOESY spectra (c) and (d) demonstrate NOE connectivities associated with S6-OH$^{\gamma}$. The resonance for S6-OH$^{\gamma}$ in (c) is identified at lower threshold.

native protein (Table 12). The data are consistent with equivalent S−O$^{\gamma}$···HN hydrogen bonds being absent in each mutant protein.

Discussion

Isolation and Characterization of Mutant Proteins. The four Cys to Ser (CtoS) mutant proteins of *Cp* Rd are expressed in *E. coli* as Zn^{II} forms. In the absence of specific incorporation mechanisms, zinc will be favored over iron in a reducing environment as, for Zn^{II} (d^{10}), there is no change in ligand field stabilization energy upon transfer of metal from M^{II}_{aq} to $M^{II}(SR)_4$ sites. In the present isolation, however, the Zn^{II} forms could be converted to iron forms at the crude lysate stage by mild denaturation followed by renaturation under reducing conditions in the presence of excess Fe^{II}. Subsequent aerial oxidation resulted in stable Fe^{III} forms.

A 49-residue N-terminal domain of a transcription factor IIB homologue from the hyperthermophilic archaeon *Pyrococcus furiosus* contains a Rd metal-binding motif and has been overexpressed in *E. coli*.[102] It was found to bind either Zn^{II} or Fe^{III}, but the zinc form is thermally more stable than is the iron form. In addition, substitution of zinc for iron has been observed for other iron proteins expressed in *E. coli*, including one only of the two $Fe(S\text{-}Cys)_4$ sites in desulforedoxin from *D. gigas*.[103]

The $Fe^{III}(S\text{-}Cys)_4$ site of *Cp* Rd exhibits a pseudo-2-fold symmetry which distinguishes pairs of interior (C6,39) and surface (C9,42) ligands (Figure 1). Comparison of the electronic and resonance Raman spectra of the four mutant proteins (Figures 5 and 6) shows that the spectra of the pairs C6S, C39S and C9S, C42S differ but are similar within each pair. It is apparent that the systematic substitution of a sulfur atom by an oxygen atom maintains similar environments for the new pairs of interior (S6,39) and surface (S9,42) side chains. As noted previously,[11] the EPR spectrum of the Fe^{III}-C42S protein exhibits resolved splitting in the ±1/2 feature (Figure 7b). ^{1}H hyperfine coupling to the paramagnetic center is a plausible explanation. However, identical EPR spectra are observed in ^1H_2O or ^2H_2O for each of the four mutant proteins, eliminating the possibility of coupling to exchangeable protons. The possibility of multiple conformations will be assessed via NMR experiments on forms substituted with the diamagnetic Ga^{III} ion.

The observations are consistent with the presence of a four-coordinate $[Fe^{III}S_3O]$ unit in each protein, derived simply from the $[Fe^{III}(S\text{-}Cys)_4]$ site of *Cp* Rd. Whether the Ser residue is bound as a ligand in a given mutant protein and, if so, whether it is protonated (ol ligand) or deprotonated (olate ligand) are not discernible from these spectra.

The reduction potential of *Cp* rRd is independent of pH. Those of the surface ligand mutants C9S and C42S are independent at pH values above a pK_a^{red} of about 7 while that of the interior ligand mutant C6S is independent above pH 9 (Figure 9). The electrochemistry becomes irreversible about 1 pH unit below pK_a^{red}. The data in Table 7 indicate that a shift

(102) Zeng, Q.; Lewis, L. M.; Colangelo, C. M.; Dong, J.; Scott, R. A. *J. Biol. Inorg. Chem.* **1996**, *1*, 162−168.

(103) Czaja, C.; Litwiller, R.; Tomlinson, A. J.; Naylor, S.; Tavares, P.; LeGall, J.; Moura, J. J. G.; Moura, I.; Rusnak, F. *J. Biol. Chem.* **1995**, *270*, 20273−20277.

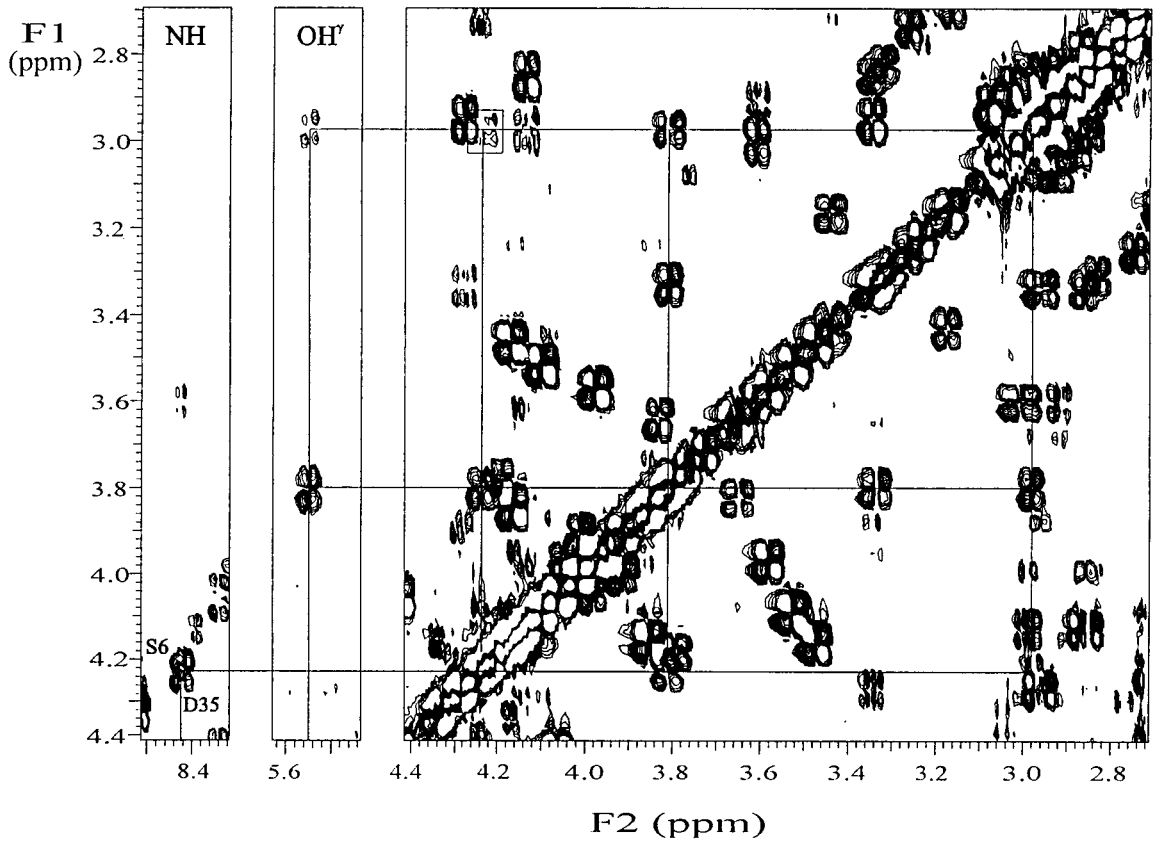

Figure 14. DQF-COSY spectrum of the C6S mutant identifying the complete S6 spin system.

Table 12. Changes in ^{1}H Chemical Shifts ($\Delta\delta$, ppm) in Cd^{II} Mutant Proteins:[a] Amide Protons Involved in NH···S Interactions in the Fe^{III}-*Cp* rRd Form

protein	V8	C9	Y11	L41	C42	V44
C6S	**−1.62**	**−1.93**	0.16	−0.12	−1.01	−0.05
C9S	−0.65	−0.55	**−1.65**	−0.45	−0.33	−0.17
C39S	0.08	−0.86	0.01	**−1.84**	*b*	0.00
C42S	−0.54	−0.85	−0.03	−0.6	0.21	**−1.65**

[a] Chemical Shift difference taken as (mutant − recombinant) in Cd^{II} forms. [b] Not identified.

in the potential of the Fe^{III}/Fe^{II} couple $E°_A$ (Scheme 1) of about −100 mV is associated with a change of interior cysteine ligands C6 and C39 to serine. The shift is doubled to about −200 mV for a change of surface ligands C9 and C42. As the electronic spectra of the Fe^{III} forms are independent of pH, the overall behavior is consistent with protonation of the Fe−O$^\gamma$-Ser link upon reduction (eq 2) with possible subsequent hydrolysis (eq 3) The following discussion explores the source of the

$$Fe^{III}-O^{\gamma}\text{-Ser} + H^+ + e^- \rightarrow Fe^{II}-O^{\gamma}(H)\text{-Ser} \quad (2)$$

$$Fe^{II}-O^{\gamma}(H)\text{-Ser} + H_2O \rightarrow Fe^{II}-OH_2 + HO^{\gamma}\text{-Ser} \quad (3)$$

differences in $E°_A$, pK_a^{red}, and electrochemical reversibility of the pairs of interior and surface ligand mutant proteins.

Fe^{III}-CtoS Mutant Proteins. The presence of an Fe^{III}−O$^\gamma$-S42 covalent bond of 1.82(8) Å is confirmed in crystals of the C42S protein grown at pH 4 (Figure 3). The major changes to the active site structure (Table 8) are consistent with (i) the relative difference in the size of an oxygen atom and a sulfur atom[104,105] and (ii) the fact that the polypeptide chain carrying interior ligands C6 and C39 is constrained by the rigid aromatic core of the protein.[5]

Consequently, significant structural change is restricted to the region around the mutation where the relative mobility of the polypeptide chain close to the molecular surface permits accommodation of the shorter FeO and CO bonds. The atoms defining the surface in this region are more closely packed as a result.

The EXAFS experiment on a frozen solution of the C42S protein at pH 4 confirms the Fe^{III}−O and Fe^{III}−S distances observed in the crystal structure (Table 10). The distances derived at pH 8 are identical, within experimental error. Equivalent results obtain for the C9S protein at pH 8 (Figure 11; Table 10) and indicate the presence of a four-coordinate [Fe^{III}(S-Cys)$_3$(O-Ser)] center in the surface ligand mutants C9S and C42S at pH 8. The near-edge spectra of the Fe^{III} forms of the interior ligand mutants C6S and C39S are also typical of pseudotetrahedral geometry. Although the difference is approaching the accuracy of the technique, the derived Fe−O distances of 1.87(1) Å for both C6S and C39S appear to be longer than those, 1.84(1) Å, of the two surface ligand mutants (Figure 11; Table 10). Such a difference would be consistent with the longer Fe^{III}−S distances observed for the interior ligands (2.29, 2.28(1) Å) compared to the surface ligands (2.25, 2.23(1) Å; Table 8). The variation can be attributed to the chain carrying the interior ligands being constrained by the rigid aromatic core of the protein.[5] However, the present EXAFS data cannot discern definitively between possible Fe^{III}−O-Ser or Fe^{III}−OH$_x$ (x = 1, 2) links in the interior ligand mutants.

Fe^{II}- and Cd^{II}-CtoS Mutant Proteins. Recent accurate mass determinations for a range of zinc proteins containing Cys_4 and

(104) Pauling, L. *The Nature of the Chemical Bond*; Cornell University Press: Ithaca, NY, 1960.

(105) Millar M.; Lee, J. F.; Koch, S. A.; Fikar, R. *Inorg. Chem.* **1982**, *21*, 4105−6.

Cys_3His active site ligand arrays have been reported.[106] The interpretation advanced suggests that two cysteinyl protons only are lost for each Zn^{II} ion bound, i.e., that these proteins exhibit $[Zn^{II}\{S\text{-}Cys\}_2\{S(H)\text{-}Cys\}_2]$ and $[Zn^{II}\{S\text{-}Cys\}_2\{S(H)\text{-}Cys\}\{N\text{-}His\}]$ centers. The question arises as to the protonation state of the reduced $[Fe^{II}S_3O]$ centers of the present mutant proteins and of their M^{II}-substituted forms, given that M^{II} species are weaker acids than M^{III} species, in general.

^1H NMR experiments on the Cd^{II}-CtoS proteins reveal the following: (i) $Cd-O^{\gamma}$-Ser bonds are present in the surface ligand mutants C9S and C42S as detected by $^{113}Cd-O^{\gamma}-CH^{\beta}_2$ coupling (Figure 12). Equivalent coupling was not detected for the interior ligand mutants. This may be due to smaller scalar couplings as these are expected to depend on the $Cd-O^{\gamma}-C^{\beta}-H^{\beta}$ dihedral angles.[89,90,92] On the other hand, the $Cd-O^{\gamma}$-Ser link may be kinetically labile[89] or, indeed, absent (cf. eqs 2 and 3). (ii) Ser-OH^{γ} protons are present in the interior ligand mutant C6S and in the surface ligand mutant C42S (Figures 13 and 14). (iii) Ser-$O^{\gamma}\cdots$HN hydrogen-bonding interactions equivalent to Cys-$S^{\gamma}\cdots$HN in rRd are absent in each mutant (Figure 1; Table 12).

The data confirm the presence of a four-coordinate $Cd^{II}(S\text{-}Cys)_3\{O(H)\text{-}Ser\}$ center featuring a $Cd-O^{\gamma}(H)$-Ser link in the C42S protein. The very similar ^1H chemical shifts observed for the serine spin systems in the C9S and C42S mutants (Table 11) indicate that an equivalent center is present in the C9S protein. This correlates with the similar H^{α} and H^{β} shifts for C9 and C42 in Cd^{II}-*Cp* rRd (Table 12). A Ser-OH^{γ} proton was detected in C6S. However, the present NMR data are not able to confirm the presence of $Cd^{II}-O^{\gamma}$-Ser bonds in the interior mutant proteins C6S and C39S.

The EXAFS data estimate $Fe^{II}-O$ distances of 1.92(2) Å for each of the surface ligand mutant proteins Fe^{II}-C9S and -C42S at pH 8. The distance increases to 2.10(2) Å at pH 6 (Table 10; Figure 11). The data are consistent with protonation or hydrolysis of the $Fe^{II}-O^{\gamma}$-Ser link (pK_a about 7), as suggested by the electrochemical data (eqs 2 and 3; Table 7). For reduced interior ligand mutants C6S and C39S, data at pH 8 match those for the surface ligand mutants at pH 6 (Figure 11). This is again consistent with electrochemical data which indicate a pK_a around 9 for the Fe^{II} forms of these mutants.

Dithionite-Treated C42S Rubredoxin. An attempt to generate crystals of the Fe^{II}-C42S protein involved treatment of crystals of Fe^{III}-C42S with sodium dithionite at pH 4. Iron was lost, and at least 1 equiv of SO_2, the oxidation product of the reducing agent SO_2^-, was incorporated into the apo protein crystals (Figure 4; Table 9). The structural model indicates that (i) the Fe^{II} form of the C42S mutant is unstable at pH 4 (it is stable at pH 6 (Table 10)), (ii) the protein tertiary structure is maintained (the Fe atom is important for function but not for overall structure), and (iii) Cys-SH functions as an effective nucleophile at pH 4.

$$\text{Cys-SH} + SO_2 \rightarrow \text{Cys-}S^{II}-S^{IV}O_2^- + H^+ \qquad (4)$$

The structural model is supported by related experiments in solution at pH 4 which are also consistent with products formed via eq 4 (Table 2). The reaction may well involve thiolate Cys-S^- as nucleophile rather than Cys-SH.[90,107,108] A cysteine persulfide residue has been detected in the Y13C mutant of ferredoxin I from *Azotobacter vinelandii*.[109]

Reduction Potentials and Proton Dissociation Constants. The factors influencing the ionization energy contribution to the reduction potential $E°_A$ of a redox site have been summarized.[14] Assume initially that the effective dielectric constant of the protein medium is the same for each mutant protein, as is the geometry of the ligand field. Then, the influences of effective nuclear charge Z'_{eff} and electronic relaxation will be the principal determinants of $E°_A$. The conversion of an Fe-$(S\text{-}Cys)_4$ to an $Fe(S\text{-}Cys)_3(O\text{-}Ser)$ site incorporates a stronger σ-donating olate ligand. This should reduce the magnitude of Z'_{eff} and decrease $E°_A$. This effect appears to drive the observed decrease in $E°_A$ of -0.5 V upon substitution of X = S by X = O in anions $[Fe^{III}(XAr)_4]^-$ dissolved in MeCN.[75] On the other hand, the substitution of Ser for Cys in *Cp* rRd should decrease the ligand character of the redox orbital of the Fe^{III} center.[14] The change in electronic relaxation effects should lead to an increase in $E°_A$. The observed decrease in $E°_A$ of 200 mV above pH 7 (Figure 9) in the surface ligand mutants C9S and C42S suggests that the Z'_{eff} factor dominates in these systems with their demonstrated $Fe^{III}(S\text{-}Cys)_3(O\text{-}Ser)$ centers at pH 8 (Figure 3; Table 10).

EXAFS measurements cannot distinguish between the possibility of $Fe^{III}(S\text{-}Cys)_3(O\text{-}Ser)$ or $Fe^{III}(S\text{-}Cys)_3(OH_x)$ (x = 1, 2) centers at pH 8 in the interior ligand mutants C6S and C39S. Their $Fe^{III}-O$ distances may be longer than those in the surface ligand mutants (Table 10), similar to the behavior of the $Fe^{III}-S$ distances in *Cp* Rd (Table 8). However, the assumption of the presence of an $Fe^{III}(S\text{-}Cys)_3(O\text{-}Ser)$ center in each mutant at pH 8 allows a simple interpretation of the total electrochemical data which are consistent with the available X-ray crystallographic and EXAFS structural data.

A longer Fe−O-Ser bond would reduce the ligand σ-donor strength, increasing Z'_{eff} and $E°_A$, correlating with the more positive $E°_A$ values of the interior ligand mutants relative to the surface ligand mutants (Table 7).

The pH dependence of the reduction potentials of the mutant proteins (Figure 9) is attributed to protonation of the O-Ser ligand following reduction (eq 2). While a free serine residue exhibits a pK_a of 13.6, a value of 7.5 is reported for a $Zn^{II}-O(H)-CR_2-$ species featuring a benzyl alcohol pendant arm attached to a quadridentate cyclen ligand.[110] Estimates derived for the Fe^{II} forms of the present mutants indicate that interior ligand S6 (pK_a^{red}, 9) is about 2 orders of magnitude more basic than are surface ligands S9 and S42 (pK_a^{red}, 7; Table 7). This observation is also consistent with a longer, weaker Fe−O-Ser link in the C6S protein (Table 10), the same structural feature used to rationalize the different $E°_A$ values.

The electrochemistry of the surface ligand mutants, C9S and C42S, is chemically reversible in the range 10 > pH > 6 and that of the interior ligand mutant C6S in the range 10.5 > pH > 7.6. The onset of irreversibility as the pH is lowered occurs 1−2 pH units below the values of pK_a^{red} (7 and 9, respectively). This behavior may be attributed to hydrolysis of the $Fe^{II}-O(H)$-Ser bond (eq 3). This proposal is again consistent with a longer, weaker Fe−O-Ser link in the interior ligand mutants and with the isolation of apo protein derivatives generated by hydrolysis upon reduction at pH 4 (cf. Table 2; Figure 4).

Inherent to the above discussion is the assumption that the effective dielectric constant is the same for each mutant protein.

(106) Fabris, D.; Zaia, J.; Hathout, Y.; Fenselau, C. *J. Am. Chem. Soc.* **1996**, *118*, 12242−12243.
(107) Wilker, J. J.; Lippard, S. J. *J. Am. Chem. Soc.* **1995**, *117*, 8682−8683.
(108) Wilker, J. J.; Lippard, S. J. *Inorg. Chem.* **1997**, *36*, 969−978.
(109) Kemper, M. A.; Stout, C. D.; Lloyd, S. E. J.; Prasad, G. S.; Fawcett, S.; Armstrong, F. A.; Shen, B.; Burgess, B. K. *J. Biol. Chem.* **1997**, *272*, 15620−15627.
(110) Kimura, E.; Kodama, Y.; Koike, T.; Shiro, M. *J. Am. Chem. Soc.* **1995**, *117*, 8304−8311.

This is obviously flawed as it implies an identical contribution to the solvent energy term.[14] The conformation of the protein chain around the mutation site in the Fe^{III}-C42S protein is different from that in the recombinant form and, presumably, from that close to the mutation site in the interior ligand mutants. These changes in the orientation of amide dipoles will influence $E°_A$.[16] In addition, there is a differential loss in the number of NH···S-Cys hydrogen bonds: two and one for the interior and surface cases, respectively (Figure 1; Table 12). The closer packing of atoms observed around the mutation site of the Fe^{III}-C42S protein indicates reduced solvent accessibility in that form. The latter effect and the loss of NH···S-Cys hydrogen bonds would both decrease $E°_A$ by stabilizing the oxidized $[Fe^{III}(S\text{-}Cys)_3(O\text{-}Ser)]^-$ center which has a lower overall negative charge than its Fe^{II} partner. What are the magnitudes of these effects relative to those induced by substitution of ligand atom O for S?

Mutant *Cp* rRd molecules have been generated in which surface Gly residues 10 and 43 (adjacent to ligands C9 and C42; Figure 1) are replaced by Ala and Val which feature more bulky CH_3 and $CH(CH_3)_2$ side chains.[10] X-ray crystal structures[111] reveal that mutation of (i) G43 to A43 increases the V44-NH···S-C42 distance to 4.0(1) Å, eliminating any possible hydrogen bond, (ii) G10 to V10 imposes steric interactions which induce the amide bond linking residues 9 and 10 in V10 mutants to invert, leading to significant structural perturbation to the chelate loop carrying the C9 ligand, and (iii) G10 or G43 reduces solvent accessibility in the Fe^{III} forms. These structural changes lead to decreases in $E°_A$ of up to 50 mV.[10] Similar shifts due to similar changes will certainly contribute in the present CtoS mutant proteins, but they would appear to be secondary to the influence of ligand atom substitution.

(111) Lavery, M. L.; Xiao, Z.; Wilce, M. C. J.; Guss, J. M.; Wedd, A. G. Manusript in preparation.

Conclusions

Differences in reduction potentials, their pH dependence, and the onset of irreversible behavior in the electrochemistry of the four CtoS mutant proteins of *Cp* Rd can be attributed to differences in the nature of $Fe-O^{\gamma}$-Ser bonds imposed by variation of the conformational flexibility of the protein chains which carry the ligands.

Acknowledgment. This work was supported by Australian Research Council Grant A29330611 to A.G.W. M.C.J.W. was supported by ARC Grant A29601726 to J.M.G. and Prof. H. C. Freeman. We thank Dr. Kerry Nugent at the University of Melbourne for recording resonance Raman spectra and Mr. Chris Noble at Monash University for recording EPR spectra. Drs. Charles Young, Ingrid Pickering, and Roger Prince are thanked for assistance with EXAFS measurements. The EXAFS work was supported by a grant from the Major Research Facilities Program of the Australian Nuclear Science and Technology Organization and by the Stanford Synchrotron Radiation Laboratory (funded by grants from the Department of Energy and the National Institutes of Health).

Supporting Information Available: A listing of negative-ion electrospray ionization mass spectra of C42S protein treated with dithionite at pH 4 (Figures S1 and S2) and NMR data (Table S1; Figure S3) (7 pages, print/PDF). See any current masthead page for ordering information and Web access instructions.

JA973162C